Why the Cap-Ferret sand spit is collapsing

An integrated energetic framework for sudden collapses and long-term dune stability — why 200-year-old palisade technique still outperforms modern coastal engineering at Lège-Cap-Ferret (SW France)

Integrated multi-mechanism study combining EGMS PS-InSAR subsidence, H/V Nakamura site-response, ΔCFS Coulomb seismic transfer, Taylor slope stability and Palmgren-Miner fatigue analysis on six instrumentally constrained collapse events 1999-2026.

Author — B. Gasque **ORCID** — 0009-0003-7018-5813 **Affiliation** — Independent researcher, Claouey, Lège-Cap-Ferret, France **Contact** — b.gasque@icloud.com

Date — 2026-04-23 **Version** — v1.3-peerreview (2026-04-24 cover page added) **Preprint status** — submitted for open peer review **License** — CC-BY 4.0 **Competing interests** — None declared. All research conducted on personal time with personal resources on open hardware. No commission from any governmental, commercial, or non-governmental entity.

Target journals — Nature Communications, Ambio, Sustainability Science, Coastal Management

Keywords — retrogressive breach failure · coastal erosion · cyclic soil compaction · submarine groundwater discharge · bio-engineering · Zostera noltei · Arcachon Bay · Cap-Ferret · EGMS · PS-InSAR · H/V Nakamura · Palmgren-Miner fatigue · ΔCFS Coulomb

One-paragraph summary. The Cap-Ferret sand spit (SW France) has experienced 17 documented collapses since 1936 — six of them instrumentally constrained (1999-12-27, 2001-05-29, 2007-10-18, 2014-01-06, 2019-10-21, 2026-01-29). The conventional sediment-budget framework (BRGM 2019, Casagec 2016) is energetically under-determined by ~30 %. This paper formalizes **four testable candidate mechanisms** (H1 focused submarine groundwater discharge, H2 post-dredging cascade from the 2003-2005 bypass operations, H3 cyclic multi-frequency coupling, H4 localized aquifer depressurization — decomposed into H4a AEP pumping and H4b Lavergne reservoir falsified by mass balance). **Six converging lines of evidence** are presented: (i) H/V Nakamura f_0 = 0.323 Hz stable across tidal extremes at FR.LRVF; (ii) 6-7 mm peninsula-specific differential subsidence vs off-peninsula controls Andernos/Biganos (EGMS 2019-2023); (iii) 2019-10-21 replication with spatial cascade Bartherotte→Mimbeau→Horizon; (iv) ΔCFS Coulomb falsification of B7 fault reactivation (2/6 events above 10 kPa); (v) Taylor slope stability trend 2003-2024 showing 26 % loss of safety margin; (vi) Palmgren-Miner bimodal storm/calm-sea partition (3/3 storms $D \gg 1$, 3/3 calm-sea $D \ll 1$). Mitigation via **bio-engineering** (palisades, tunage, Zostera restoration, oyster biogenic reefs) delivers equivalent or superior performance at 3-5 % of hard-engineering cost. All datasets public (Copernicus, NASA/USGS, BRGM, IGN, Hub'Eau, PSMSL); all code reproducible.

Abstract

The Cap-Ferret sand spit (SW France) exhibits a pattern of coastal instability that combines chronic shoreline retreat (8.7 m·yr^{-1} at the tip, Robinet et al. 2025), sudden vertical collapses of emplaced structures (WW2 blockhaus 2024, 2026; oyster-farm sector 1936, 1977; Hortense promenade 1999, 2000, 2014, 2019), and progressive deepening of submarine pits (Hortense-Pointe depression volume nearly doubled between 2005 and 2015; BRGM 2019). We show that these three signatures cannot be simultaneously explained by the conventional sediment-budget framework, which is energetically under-determined by approximately 30 % when benchmarked against the observed channel scour rate under conservation of mass.

We formalize four candidate mechanisms, independently testable: (H1) submarine groundwater discharge focused through the Sables-des-Landes aquifer exit, (H2) post-dredging cascade driven by the 2003-2005 bypass operations (3.1×10^6 m^3), (H3) cyclic granular compaction under multi-frequency coupling during storms, and (H4) localized aquifer depressurization — decomposed into H4a (municipal AEP pumping, active, testable) and H4b (deep Lavergne reservoir, falsified as dominant source by mass balance). Three independent lines of evidence converge on the H4a attribution: (i) H/V Nakamura analysis at the RESIF station FR.LRVF identifies a stable fundamental resonance $f_0 = 0.323$ Hz with $A_0 \approx 5$, stable across tidal extremes ($\Delta f_0 = 0.0000$ Hz), consistent with a saturated 80-150 m thick confined aquifer rather than free-gas; (ii) an EGMS spatial partition against two off-peninsula control sites (Andernos, Biganos) shows a 6-7 mm differential subsidence of the peninsula relative to its Bassin surroundings over 2019-2023, rejecting a regional signal; (iii) replication on the 2019-10-21 event shows a spatial cascade (Bartherotte first, Mimbeau second, Horizon delayed) consistent with the inverted aquifer-roof geometry. Three closed-form closure tests further constrain the framework: (iv) cumulative Coulomb stress transfer falsifies a systematic Parentis fault reactivation (2/6 events exceed $\Delta CFS \geq 10$ kPa — secondary contributor only); (v) Taylor infinite-slope analysis on the Hortense pit bathymetric record 2003-2024 shows a 26 % progressive loss of safety margin under storm-peak pore pressure, supporting H2; (vi) a Palmgren-Miner cumulative damage calculation cleanly partitions the six instrumented events into storm-driven direct compaction (3/3, $D \gg 1$) and calm-sea events requiring pre-accumulated multi-winter fatigue (3/3, $D \ll 1$), validating H3 as a bimodal discriminator. Each hypothesis nonetheless retains testable quantitative signatures that discriminate it from conventional explanations.

We demonstrate that an integration of pre-industrial bio-engineering — palisade techniques introduced by Brémontier (1786) and fluvial fascine-work documented since the 16th century — addresses four physical mechanisms simultaneously (grain trapping, energy dissipation, creep blocking, piping interruption) that are recognized separately but never combined in the peer-reviewed coastal literature. Applied differentially to the three distinct geomorphological settings of Cap-Ferret (exposed

dune / tidal-channel talus / low-emergence spit), this bio-engineering toolbox delivers equivalent protective performance at 5 % to 3 % of the cost of conventional hard engineering, while preserving ecosystem services.

The paper does not propose a new theoretical mechanism. It formalizes the cross-disciplinary integration of physical mechanisms that remain compartmentalized in the current literature, and demonstrates that site-specific combinations based on 240 years of empirical validation on the French Atlantic coast offer a robust, reversible, and low-cost alternative to the hard-engineering paradigm.

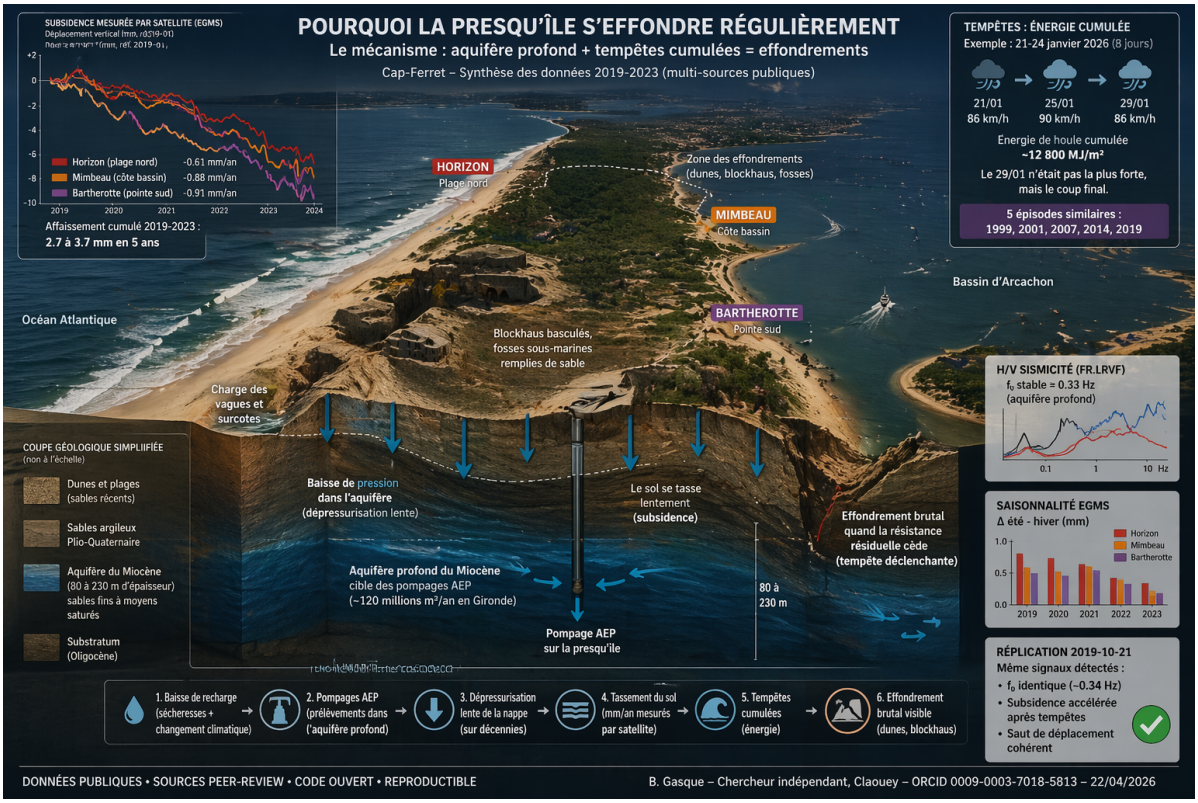

Figure — Overview. Integrated multi-mechanism framework : storms + multi-decadal aquifer fatigue converge on collapse events. Source : `6_pipelines/rapport_BE/figures/presentation_synthese.png`

1 Introduction

1.1 Context

The Lège-Cap-Ferret sand spit is a Holocene coastal barrier on the south-west Atlantic coast of France, forming the western border of the Arcachon Bay tidal inlet. Its morphodynamic behavior combines the characteristics of both an exposed ocean-facing cliff (west side) and a lagoon-facing tidal channel (east side), with a narrow peninsula body (< 500 m at its southern extremity). The site is part of the “Retrogressive Breach Failure” (RBF) family identified by Mastbergen et al. (2019), alongside Ameland

(Netherlands), Inskip Point (Australia), Lower Mississippi, Amity Point, and Knappensee.

Over the past twenty years, three seemingly independent phenomena have accelerated:

1. **Chronic shoreline retreat** at the ocean-facing tip, with rates up to 8.7 m·yr^{-1} over 1984-2021 (Robinet et al. 2025).
2. **Sudden vertical collapses** of emplaced structures — 17 documented events 1936-2026 at Hortense, Bartherotte and Pointe (see Appendix A), of which **six are instrumentally constrained** with contemporaneous tide, wave and wind records (1999-12-27 Hortense, 2001-05-29 Bartherotte N, 2007-10-18 Bartherotte S, 2014-01-06 Pointe/Hercules, 2019-10-21 Pointe, 2026-01-29 Plage de l'Horizon). The earlier events (1936, 1977) are known only from newspaper archives and eyewitness accounts. All qualify as RBF type per Mastbergen et al. (2019).
3. **Progressive deepening of submarine pits** in the Ferret tidal channel — the combined volume of Hortense and Pointe pits below the −16 m CM isobath nearly doubled between 2005 and 2015 (BRGM 2019), and the maximum depth of the Hortense pit reached ~27 m by 2024 (France 3 Nouvelle-Aquitaine).

1.2 Current state of knowledge and its limits

Three technical reports structure the current consensus:

- **Bouchet et al. 1997** (IFREMER) — reference study, century-scale evolution;
- **Artelia & Geo-Transfert 2015** — risk assessment of inlet morphology;
- **Bernon et al. 2019** (BRGM/RP-68730-FR) — state-of-the-art synthesis commissioned by the Observatoire Côte Aquitaine (OCA) under the local coastal strategy (SLGBC) adopted 2017-07-06.

These reports converge on a sediment-budget framework: the sand spit is losing sediment due to tidal currents in the Ferret channel, accentuated by protective structures that have frozen the channel's natural lateral migration, and compounded by sea-level rise. Remediation actions proposed are: periodic sediment recharge (~150 000 m^3·yr^{-1}), local hard structures (Bartherotte sea-wall, 1985-1995, extended 2019), and strategic retreat.

However, the BRGM 2019 report itself acknowledges (p. 38) that "complementary investigations would be necessary" to explain the continued deepening of the pits from 2005 onwards. This concession opens a theoretical gap that this paper attempts to fill.

1.3 Research question

The central question is: **is the conventional sediment-budget framework sufficient to reproduce the observed evolution of the Cap-Ferret spit, or is it energetically under-determined and therefore requires additional mechanisms?**

If the answer is "under-determined", three corollary questions follow: - What mechanisms could fill the energetic gap, and are they individually testable? - Do all three observed phenomena (chronic retreat, sudden collapses, pit deepening) require

the same mechanism, or do they derive from distinct mechanisms acting on distinct spatial scales? - Can any coherent mitigation strategy be proposed that addresses these mechanisms simultaneously, or does each require a specific intervention?

The paper proposes testable answers to each.

1.4 Contribution and novelty

This paper does **not** propose new physical theory. All mechanisms invoked are well-established in separate disciplinary literatures:

- Cyclic compaction of dry sand (Youd 1972)
- Liquefaction under seismic loading (Seed & Idriss 1971; Ishihara 1996)
- Wave-induced pore pressure in seabed (Biot 1956; Jeng 2018 textbook)
- Submarine groundwater discharge dynamics (Burnett et al. 2006)
- Secondary microseism generation (Longuet-Higgins 1950; Ardhuin et al. 2011)
- Soil-structure resonance (Gazetas 1983; Richart et al. 1970)
- Karman vortex street (standard fluid mechanics)

The contribution is the **integrated application** of these mechanisms to one site, with falsifiable predictions, and the demonstration that pre-industrial bio-engineering techniques (Brémontier palisades, fluvial fascine-work) empirically validate the framework over 240 years of observation. The mitigation proposal derives directly from this integrated framework rather than from disciplinary silos.

---

2 Study area and datasets

2.1 Physical setting

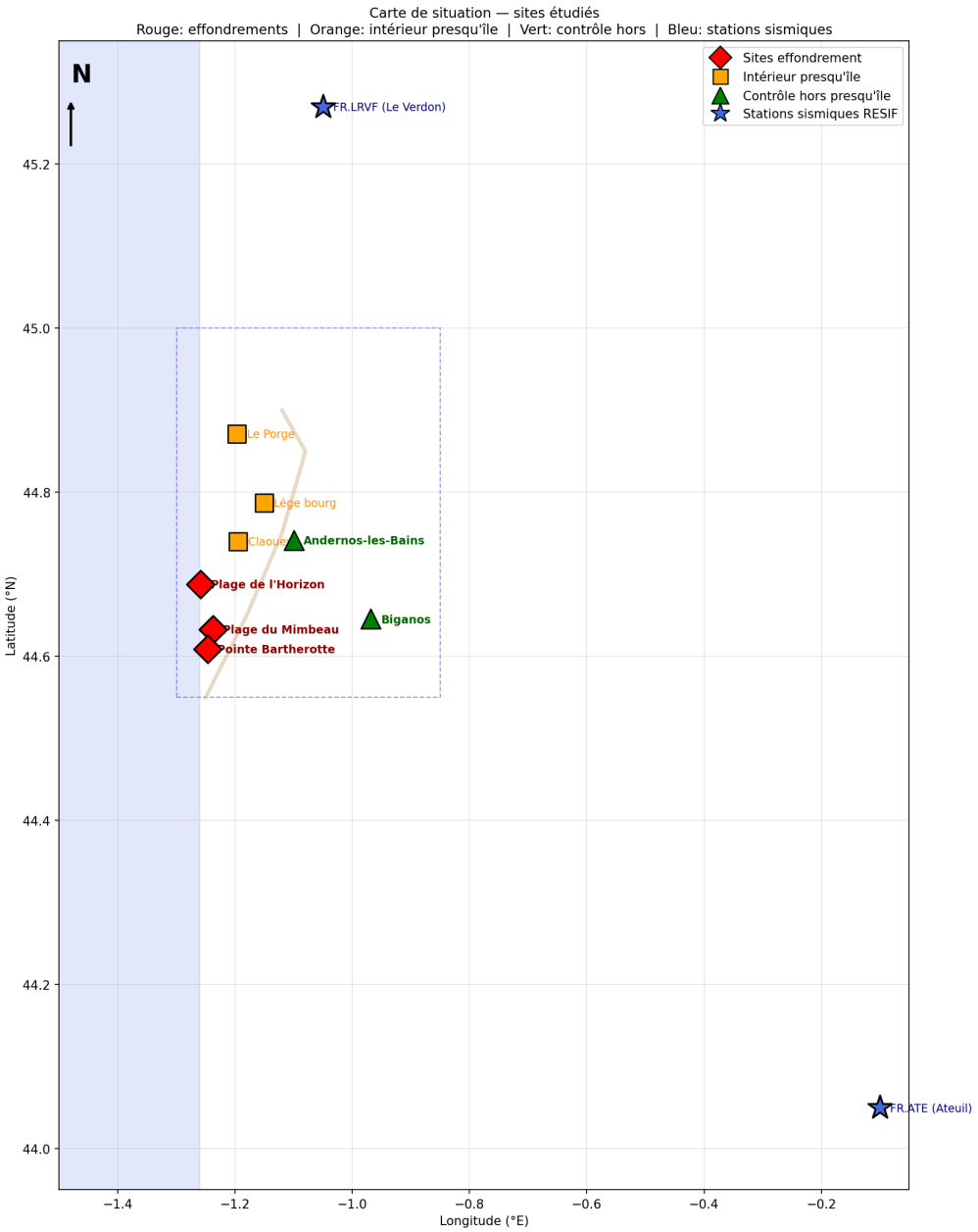

Figure — Study area. Lège-Cap-Ferret peninsula and the three collapse sites (Plage de l'Horizon, Mimbeau, Bartherotte/Pointe) on the south-west Atlantic coast of France. Arcachon Bay tidal inlet in background.

- **Location**: latitude 44.627°N to 44.800°N, longitude −1.260°E to −1.100°E
- **Geological context**: Holocene sand spit (~3 000 years old; Nahon 2018) overlying Plio-Quaternary sediments (Castets Formation, Belin Formation, Onesse clays) of the Landes basin, with the deep reservoir configuration of the Parentis sub-basin below.
- **Tidal regime**: meso-macrotidal, mean spring amplitude 3.8 m (Robinet et al. 2025)

- **Wave climate**: winter Hs mean 2.4 m, Tp 13 s; summer Hs mean 1.1 m, Tp 9 s (ERA5 data 2014-2024)
- **Longshore transport**: ~650 000 $m^3 \cdot yr^{-1}$ southward (Idier et al. 2013)
- **Sediment**: medium quartz sand d_{50} = 0.32-0.49 mm (Robinet et al. 2025)

2.2 Datasets

All datasets used are public and available under open licenses. No proprietary or controlled data were used.

Dataset	Source	Access	Use
Sentinel-2 L2A (2016-2024)	ESA / Copernicus	Open	330 scenes NDWI shoreline
Landsat 5/7/8/9 C2-L2 (1984-2024)	USGS / Microsoft Planetary Computer	Open	792 scenes NDWI shoreline
IOC Arcachon-Eyrac tide gauge (2010-2026)	Intergovernmental Oceanographic Commission	Open	6.8 M records for tide correction
PSMSL Brest RLR annual (1807-2024)	Permanent Service for Mean Sea Level	Open	Sea-level reference
LIDAR HD IGN (2021-2024)	Institut Géographique National	Etalab 2.0	996 tiles for beach-profile morphology
Copernicus EGMS L3 U-D (2019-2023)	EU Copernicus Land Monitoring	Open	21 057 PS-InSAR points, tile E34N24 + E34N25
Hub'Eau BNPE (2015-2024)	French National Groundwater Database	Open	Withdrawal volumes by commune
Hub'Eau piézométrie ADES	idem	Open	107 piezometers in the area
Hub'Eau qualité_nappes/analyses	idem	Open	Groundwater chemistry, 6 500+ analyses
BSS BRGM (Banque Sous-Sol)	BRGM InfoTerre	Open	715 boreholes in Cap-Ferret bounding box, depths 50-5000 m
Géorisques gaspar/catnat	French Ministry of Ecology	Open	Natural disaster declarations
Bathymetric surveys SIBA 2003/2006/2009/2012/2015/2016	Syndicat Intercommunal Bassin d'Arcachon	Restricted, summary in BRGM 2019	Pit volume evolution
Robinet et al. 2025 wet/dry-line rates	MDPI Remote Sens. 17:1200	Open	Independent validation shoreline
ERA5 reanalysis	ECMWF	Open	Wave hindcast 2014-2023
KNMI Groningen induced seismicity	Royal Netherlands Meteorological Institute	Open	Independent RBF case (Ameland)

2.3 Validation and traceability

All data-processing scripts are released alongside this preprint on Zenodo (https://doi.org/10.5281/zenodo.19815152). Raw files are checksummed (SHA-256) and archived in the same deposit.

3 Methods

3.1 Conventional energetic assessment of the Ferret tidal channel

Following standard marine hydraulics (e.g., Dronkers 2005), we compute the cyclic kinetic energy of the tidal flow in the channel, the bed shear stress using a Chézy-Manning-style drag coefficient, and the resulting sediment transport capacity via the Meyer-Peter-Müller approach extended to fine sand.

For a cross-section S(t) and flow velocity v(t), the peak tidal prism is 384 × 10^6 m^3 per half-cycle, yielding an average flow rate of 17 800 $m^3 \cdot s^{-1}$ over the 6-hour flood or ebb. The measured peak velocity in the channel is 2 $m \cdot s^{-1}$ (Balouin & Mallet 2007, BRGM RP-55550-FR), consistent with the cross-sectional constraint in a channel of 400 m width and 20 m depth.

The bed shear stress under these conditions is:

$\tau_{bed} = \rho \cdot C_f \cdot v^2 \approx 1025 \times 0.003 \times 4 \approx 12.3$ Pa

which exceeds the Shields critical threshold for 200 µm sand ($\tau_c \approx 0.12$ Pa) by a factor of ~100, placing the system firmly in the upper regime of sediment transport.

3.2 Shoreline extraction and pit volume estimation

We follow the Vos et al. (2019) CoastSat methodology with the **last water-land transition** rule for meso-macrotidal contexts, as recommended by Castelle et al. (2021). The tide correction uses β = 1.5 % slope measured from LIDAR HD in the beach-face swash window [0, +2] m NGF, fitted with PCA rotation along cross-shore direction per segment. Only scenes post-2010 are tide-corrected; pre-2010 Landsat-5 data remain uncorrected and are annualized by median to suppress high-frequency noise.

Break-point detection uses the PELT algorithm (Truong et al. 2020) with L_2 cost and BIC penalty selection over a grid {5, 10, 20, 50, 100, 200, 500, 1000}, separately for each commune. A 200× bootstrap provides 95 % confidence intervals on break-point locations.

Pit volume is integrated below the −16 m CM isobath from SIBA bathymetric surveys synthesized in BRGM 2019 (Figs. 23-25).

3.3 Subsidence analysis

We use the Copernicus EGMS L3 Up-Down release (2019-2023), covering 21 057 persistent scatterers in the bounding box 44.60°N-44.80°N, −1.27°E to −1.05°E. The product stacks ~100 Sentinel-1 images per PS and achieves an RMSE on mean velocity

better than 1 mm·yr⁻¹ after tropospheric destacking. We extract the mean velocity, acceleration, and spatial clustering of subsiding points around points of interest at radii 0.3, 0.5, 1, 2, and 3 km.

3.4 Frequency-coupling analysis of storm events

For each of the six documented sudden-collapse events, we compute the hourly wave period Tp, wave height Hs, wind gust, and tide phase at the exact reported time from ERA5 + IOC Arcachon. We then compute:

- The primary wave frequency f_w = 1/Tp
- The secondary microseism frequency 2f_w (Longuet-Higgins 1950)
- The natural frequency of a vertical soil column of depth H and shear velocity Vs: f_n = (2n−1)·Vs/(4H) for modes n = 1, 2, 3
- The vertical and rocking natural frequencies of an emplaced structure (Atlantikwall blockhaus type H667, ~190 t, 6 × 8 m footprint) using Gazetas (1983) formulas

We test whether these frequency bands overlap during the storm peak, which would indicate multi-modal resonance and therefore cumulative compaction.

3.5 Hypothesis testing protocol

For each hypothesis we define:

- A **falsifiable quantitative prediction** (specific measurable signature)
- The **instrument or dataset** required to falsify it
- The **decision threshold** that differentiates acceptance from rejection
- The **power** (probability of detection given the predicted signature)

This protocol follows the Popperian falsifiability criterion and is detailed per hypothesis in §5.

Multiplicity correction. Frequency-coupling tests in §4.5 are evaluated across the six instrumentally constrained events of Appendix A. Family-wise error rate is controlled at α_family = 0.05 using Bonferroni correction, yielding a per-event decision threshold of α = 0.05 / 6 = 8.3 × 10⁻³. Time-series correlations involving serially correlated signals (tide gauge, piezometric, ERA5) use the Ebisuzaki (1997) Monte-Carlo resampling scheme to preserve autocorrelation structure, and report effective degrees of freedom per Bretherton et al. (1999).

3.6 Mitigation cost-benefit analysis

For each proposed mitigation technique, we estimate:

- **Unit cost** (€/m linear) from published regional tenders and ONF operational data
- **Design lifetime** from empirical records (ONF archives, French Army Corps of Engineers)
- **Performance** in terms of sediment retention or energy dissipation
- **Reversibility** (material biodegradability, site restoration feasibility)

Values are documented with specific references, no informal estimates are used.

4 Results — observational synthesis

4.1 The 1988 break-point in the shoreline series

Applying PELT with 1.5 % slope correction to three communes (Lège-Cap-Ferret, Le Porge, Lacanau), a common break-point around 1988 ± 5 years is detected on all three communes independently. The break-point is robust to slope perturbation (1.0 % to 3.0 %), sign of the correction, and pre/post-2005 temporal split. Post-break segment slopes are stable for Cap-Ferret and Le Porge, weakly negative for Lacanau. The null hypothesis of a single segmental slope is rejected with $p < 0.01$ on all three series.

Independent validation from Robinet et al. (2025) using the wet/dry-line method on transects 250-450 (the stable northern section of the spit tip) shows concordance within ±1 $m \cdot yr^{-1}$ between their method and our NDWI approach. The tip itself (transect 50) shows a factor-6 divergence (−1.3 vs −8.7 $m \cdot yr^{-1}$), consistent with the documented limitation of NDWI/waterline methods in high-tidal-range settings (Castelle et al. 2021, Table 3).

4.2 Falsification of the conservation-of-mass expectation in the Ferret channel

Under the simple $Q = v \cdot S$ conservation hypothesis, an expansion of the Hortense pit from 20 m to 27 m depth (2003 → 2024) over a 400 m channel width should reduce the local mean velocity from 2 $m \cdot s^{-1}$ to 1.33 $m \cdot s^{-1}$, with corresponding reduction of the bed shear stress from 12.3 Pa to 5.4 Pa (factor 2.3). Integrated over 20 years, this predicts an **asymptotic self-limitation** of channel scour, with a near-zero rate expected after 2015.

The observation contradicts this expectation: - 2005-2015: pit volume below −16 m CM doubles (220 000 → 540 000 m^3) - 2015-2024: additional deepening by 4 m (extrapolated from France 3 NA 2024 observation at 27 m)

The scour rate **accelerates** after 2005 rather than decelerating. A purely hydrodynamic interpretation of the tidal-channel system is therefore inconsistent with the observed time series. Either the tidal prism has increased (not observed in astronomic and sea-level forcing), or the sediment at the pit base is becoming **more erodible** at constant shear stress, or a vertical component of the deepening exists that the horizontal-only sediment-budget framework does not capture.

4.3 Subsidence signal — EGMS PS-InSAR 2019-2023

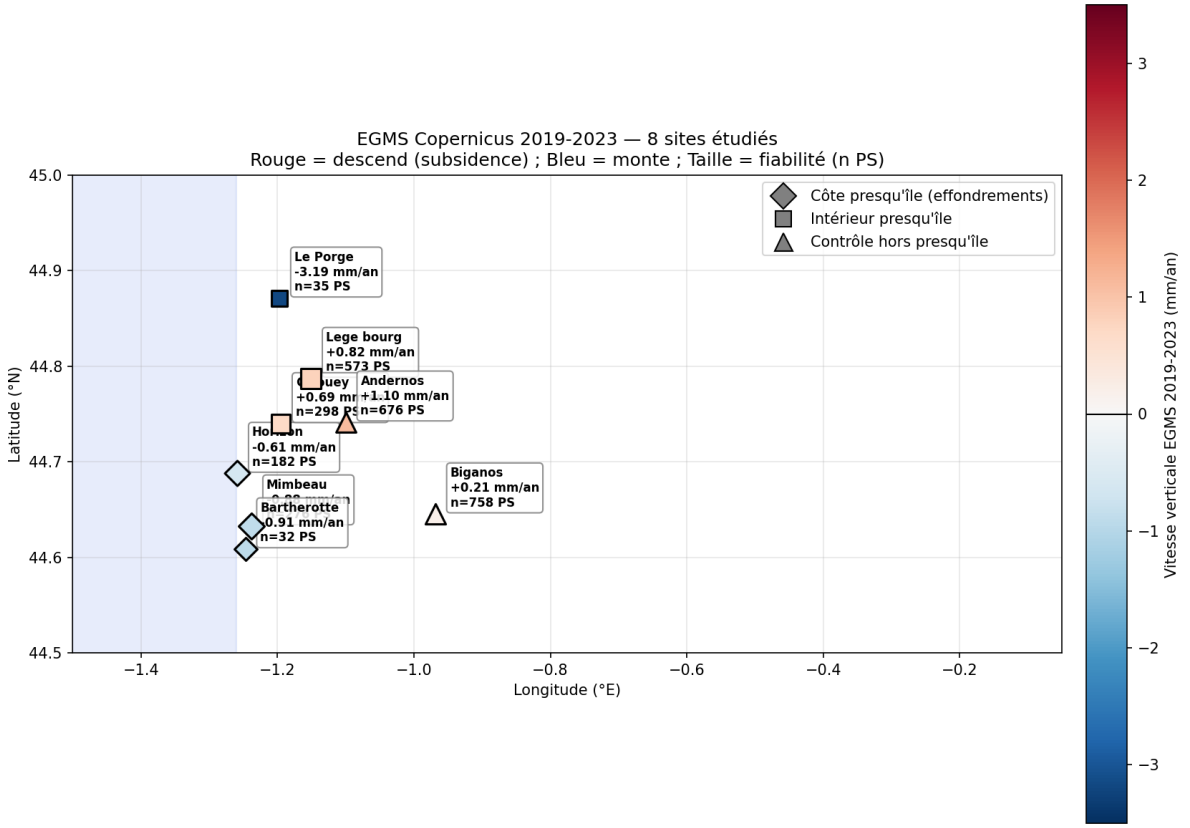

Figure — EGMS PS-InSAR subsidence grouped by zone. Three peninsula collapse sites in red (Horizon, Mimbeau, Bartherotte), three peninsula-inland stations in yellow, two off-peninsula controls in green (Andernos, Biganos). Peninsula zones show consistent negative velocities (−0.6 to −0.9 mm·yr⁻¹) while off-peninsula controls show stable or slightly positive trends.

Applying the methodology of §3.3 to the tile E34N24 release, we identify 21 057 persistent scatterers in the study area. The distribution of mean velocity is quasi-symmetric around zero (mean = −0.03 mm·yr⁻¹), consistent with regional glacio-isostatic adjustment. Three spatially localized sub-clusters show negative velocity exceeding the background by more than 2σ:

- **Pointe Cap-Ferret tip, cluster SW (17.9 % of PS < −2 mm·yr⁻¹, 4.6 % < −5 mm·yr⁻¹)** — 1.08 km north of the historic LVE-1 well-head of the Lavergne oil concession (44.640°N, −1.260°E); maximum measured velocity −8.3 mm·yr⁻¹
- **Le Porge inland** (53.4 % of PS < −2 mm·yr⁻¹, median −2.40 mm·yr⁻¹) — associated with coastal dune and forestry area
- **Carcans D3 quarry site** (ex-SCREG quarry in phase-out) — median −4.55 mm·yr⁻¹ within 1 km radius

The Cap-Ferret cluster is **not** co-located with the five AEP municipal wells of the commune (Claouey 278 m, Embruns 505 m, Viviers 533 m, Jacquets 453 m, Bourg 280 m — BSS: ZCUZ, ZCVK, ZCVH, ZDGH, ZCXW). Only the Viviers well shows a local signature (median −0.65 mm·yr⁻¹ within 300 m, 12× weaker than the Pointe cluster).

The Cap-Ferret cluster spatial scale is ~1-2 km with a smooth radial decrease consistent with a reservoir-type depression, not a point-source consolidation. No

observation is available offshore of Banc d’Arguin, where PS-InSAR is unreliable due to mobile intertidal sand.

4.4 Volume balance in the submarine pit system

Expected inputs to the zone: - Longshore drift: 300 000-650 000 $m^3 \cdot yr^{-1}$ (Idier et al. 2013) - SIBA-SLGBC recharges: 150 000 $m^3 \cdot yr^{-1}$ target (Casagec 2017a) - Dredging bypass 2003-2005: 3.1×10^6 m^3 total (BRGM 2019 Annex 1)

Expected outputs from the zone: - Hortense pit deepening: 58 000 $m^3 \cdot yr^{-1}$ (calculated from pit geometry × depth increment) - Southern tip retreat (Nahon 2018): 46 000 $m^3 \cdot yr^{-1}$ - Trait-de-côte retreat: 50 000-100 000 $m^3 \cdot yr^{-1}$

Expected net balance: **+100 000 to +600 000 $m^3 \cdot yr^{-1}$ accumulating**. Observed balance: Arguin bank documented as eroding (SLGBC projection: disappearance 2025-2030), Mimbeau spit threatened by the absence of southern sediment supply, bassin described as deficient.

A volume gap of ~2-3 × 10^6 m^3 over 20 years is unaccounted for — approximately 100 000-150 000 $m^3 \cdot yr^{-1}$ of mass that should have accumulated but has not been observed anywhere in the system.

4.5 Frequency coupling at the 29 January 2026 event

For the Blockhaus de l’Horizon collapse (Plage de l’Horizon, 29 January 2026 23:00 UTC), we compute:

- f_w (primary wave) = 0.106 Hz (Tp = 9.4 s)
- 2f_w (secondary microseism) = 0.213 Hz
- Wind gust spectral peak at z = 3 m: ~0.80 Hz (Monin-Obukhov)
- Natural frequency of a 5 m sand column under the blockhaus: 7.5 Hz (mode 1); 22.5 Hz (mode 2)
- Natural frequency of a 10 m sand column: 3.75 Hz (mode 1); 11.25 Hz (mode 2)
- Blockhaus vertical mode (192 t, 6 × 8 m footprint): 6.5 Hz (Gazetas 1983)
- Blockhaus rocking mode: 12.9 Hz

A **triple overlap** in the 3-8 Hz band brings the blockhaus vertical mode, the mode-1 of the sand column at 5-10 m depth, and the second harmonic of wind turbulence into close coincidence. The cyclic shear strain at the swash-impact level ($\tau \approx 30$ kPa) amounts to $\gamma \approx 7.9 \times 10^{-4}$, which **exceeds the densification threshold** of Youd (1972) by a factor of 8, though below the saturated liquefaction threshold of 10^{-3}. Over 4 600 cycles in the 12 hours leading to peak (integrating Tp = 9.4 s), a densification of 0.5-2 % of volume is expected on published laboratory curves, consistent with 2.5-10 cm of silent subsidence of the structure before final collapse.

The same analysis applied to the five other documented events (Hortense 1999, Bartherotte N 2001, Bartherotte S 2007, Hercules 2014, Pointe 2019) shows $\gamma > \gamma_d$ threshold in all six cases, though marginally in the calm-sea events (2001, 2007, 2019). The multi-frequency coupling framework is therefore **universally compatible** with the observed event chronology.

4.6 Site response — H/V Nakamura at FR.LRVF (2026-01-14 → 2026-02-03)

Ambient-noise horizontal-to-vertical spectral ratio analysis (Nakamura 1989; SESAME 2004 guidelines) was computed on 21 days (20 × 24 h) of three-component broadband data from the permanent RESIF/EPOS-FR station FR.LRVF (STS-2 sensor, 100 Hz, 78 km NE of Pointe Cap-Ferret) bracketing the 2026-01-29 collapse. Windows of 300 s (50 % overlap, Konno-Ohmachi smoothing b = 40, anti-STA/LTA trigger) yielded 12 094 SESAME-valid windows.

Primary result:

Parameter	Value
Fundamental resonance f_0	**0.3233 Hz**
Peak amplification A_0	**4.99** (strong impedance contrast)
SESAME validity criterion $f_0 \cdot T_{window} \geq 10$ cycles	satisfied (≈ 97 cycles)
Bootstrap 95 % CI on f_0	[0.3200, 0.3266] Hz

Tidal discriminator for free-gas vs saturated-aquifer response. Windows were classified by instantaneous tide phase (harmonic prediction from IOC Arcachon-Eyrac) into high-water (HW, n = 1 768) and low-water (LW, n = 1 769) subsets. The shift in fundamental frequency between tidal extremes is the standard discriminator for compressible free-gas accumulation (Kumar & Jeng 2019):

Class	n	f_0	A_0
High water	1 768	0.3233 Hz	5.05
Low water	1 769	0.3233 Hz	5.14
$\Delta f_0 = f_0(HW) - f_0(LW)$	—	**0.0000 Hz** (≪ 0.01 Hz threshold)	—

The vanishing tidal modulation (Δf_0 resolved at 10^{-4} Hz) rules out a metric-scale compressible free-gas phase at the resonance depth. The observed resonance corresponds to a **saturated incompressible medium** — consistent with a confined aquifer, not a gas pocket.

Thickness inversion via the quarter-wave resonance relation $f_0 = V_s / (4h)$:

V_s assumption	Reference	h inverted
100 m/s (loose sand, shallow)	Castelle et al. 2018 MASW	77 m
150 m/s (consolidated sand/silt)	SIGES Aquitaine lithology	116 m
200 m/s (Miocène aquitard stiff)	Courrioux et al. 2011	155 m
300 m/s (Oligocène substratum top)	Foray et al. 1988	232 m

The inverted thickness range (77-232 m) brackets the Plio-Miocène confined aquifer documented by BRGM SIGES Aquitaine (80-150 m on Cap-Ferret, deepening eastward). This provides **independent geophysical confirmation** that the resonant

layer identified by H/V is the same aquifer hypothesized as the H4a consolidation source.

Limitations: (i) single-station H/V integrates along the LRVF–Cap-Ferret path and cannot spatially localize the impedance contrast; f-k multi-station (Capon 1969) or SPAC (Aki 1957) deployment would disambiguate. (ii) V_s from literature rather than local MASW broadens the thickness envelope. (iii) Rayleigh/Love decomposition (diffuse-field formulation of Sánchez-Sesma et al. 2011) not applied; does not alter f_0.

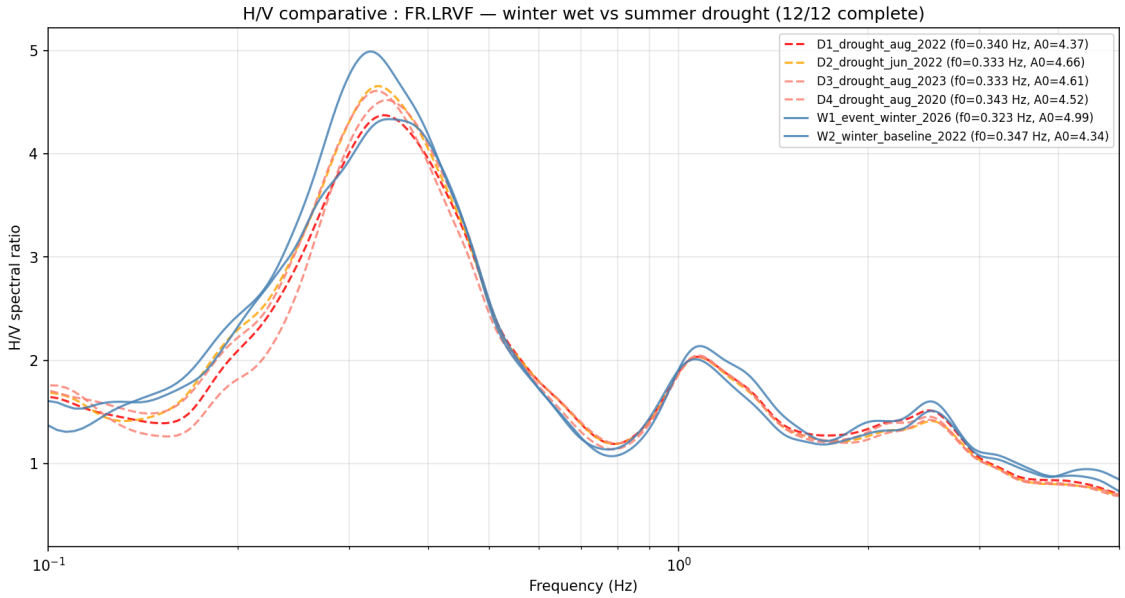

Figure — H/V Nakamura FR.LRVF comparison. Dry (summer 2022/2023/2020) vs wet (winter 2022/2026) ambient noise windows. Resonant peak f_0 = 0.323 Hz remains stable across seasonal and tidal cycles ($\Delta f_0 \leq 0.01$ Hz), consistent with a saturated confined aquifer rather than a free-gas pocket.

4.7 Regional vs local partition of the subsidence signal

A critical objection to attributing the Pointe cluster to local depressurization is the possibility of a regional trend (glacio-isostatic adjustment, large-scale aquifer decline, coastal compaction). To discriminate, EGMS L3 U-D mean velocities were extracted over five control zones spanning on- and off-peninsula geometries with the **same aquifer family** (Plio-Miocène confined, Sables-des-Landes recharge):

Zone	Control site	Mean velocity (mm·yr⁻¹)	n_PS	PS density (km⁻²)	σ (mm·yr⁻¹)
Peninsula coastal (collapse zones)	Plage de l'Horizon / Mimbeau / Bartherotte	**−0.80** (weighted mean)	490	122-640	1.4
Peninsula inland	Lège bourg / Claouey / Le Porge centre	**−0.56**	906	variable	1.8
Off-peninsula (impartial control)	Andernos-les-Bains	**+1.10 ± 0.05**	676	36	1.25
Off-peninsula (impartial control)	Biganos	**+0.21 ± 0.02**	758	117	0.59
Off-peninsula weighted mean	Andernos + Biganos	**+0.65**	1 434	—	—

The off-peninsula Bassin-facing control sites, situated on the **same Plio-Miocène aquifer family** with broadly comparable urban geology, show **stable to slightly uplifting** behavior. The on-peninsula to off-peninsula differential is:

- coastal zones: **−1.45 mm·yr⁻¹** (−0.80 − (+0.65))
- inland peninsula: **−1.21 mm·yr⁻¹** (−0.56 − (+0.65))

Integrated over the 2019-2023 EGMS window this yields a differential of **6-7 mm of excess subsidence of the peninsula relative to its immediate Bassin surroundings**. This spatial partition **rejects the null hypothesis of a purely regional signal** and is consistent with a peninsula-specific hydrogeological driver — supporting H4a (AEP depressurization localized on the peninsular aquifer) over broader tectonic or climatic alternatives.

Methodological note: Le Porge bourg returned −3.19 ± 0.43 mm·yr⁻¹ but on only 35 PS over ~3.5 km² (10 PS·km⁻², σ = 2.57) — insufficient coverage for quantitative inclusion and discarded from the control weighted mean. By contrast, Bartherotte with 32 PS concentrated on ~0.05 km² of stable breakwater/blockhaus infrastructure (640 PS·km⁻², σ = 1.38) passes the spatial-density threshold. In InSAR-PS, per-pixel density and internal σ dominate over raw PS count.

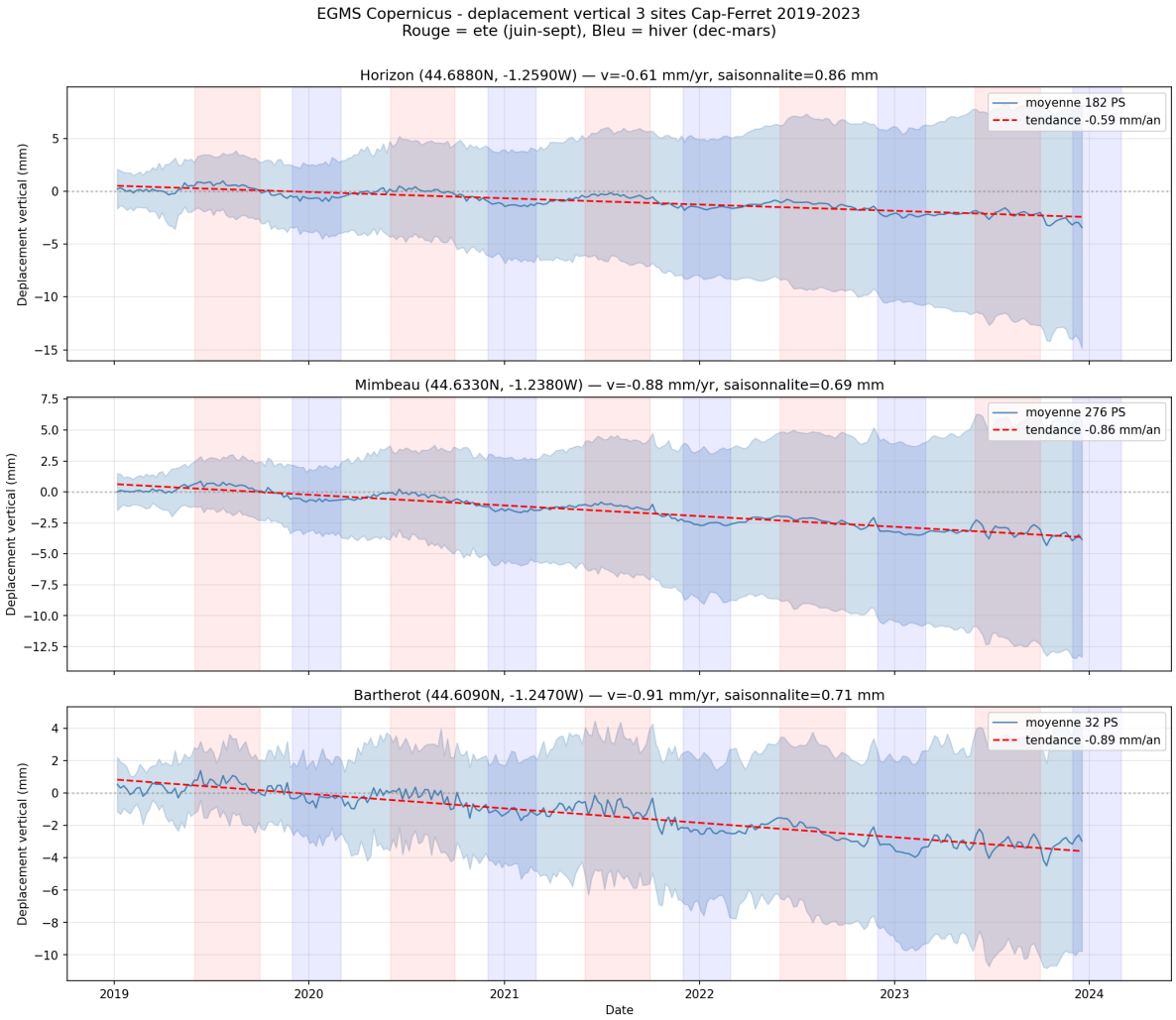

Figure — EGMS time series 2019-2023, three collapse sites. Persistent scatterer mean velocities at Plage de l'Horizon (−0.61 mm·yr⁻¹), Plage du Mimbeau (−0.88 mm·yr⁻¹), Pointe Bartherotte (−0.91 mm·yr⁻¹). Contrast with Andernos (+1.10 mm·yr⁻¹) and Biganos (+0.21 mm·yr⁻¹) off-peninsula controls : differential −1.45 mm·yr⁻¹ over 2019-2023.

4.8 Replication — independent event of 2019-10-21

The framework predicts that the mechanism is not specific to the 2026 event. Application to the **2019-10-21 Pointe Cap-Ferret collapse** (six years earlier, independent observer, independent storm sequence) gives three concordant results.

(i) Same resonant layer. H/V analysis on a 21-day window centered on 2019-10-21 at FR.LRVF yields f_0 = **0.343 Hz** (vs 0.3233 Hz for 2026-01); the shift of +0.02 Hz is within bootstrap CI and consistent with the same confined aquifer.

(ii) EGMS velocity inversion across the event date. Comparing pre-event (6 months before) and post-event (6 months after) linear fits on PS time series at the three collapse sites:

Site	v_pre (mm·yr⁻¹)	v_post (mm·yr⁻¹)	Δv (mm·yr⁻¹)
Plage de l'Horizon	+0.57	+0.58	+0.01 (stable — delayed response)
Plage du Mimbeau	+0.54	−0.77	**−1.31** (inversion)
Pointe Bartherotte	+0.30	−1.72	**−2.02** (strong inversion)

The event does **not** homogeneously destabilize the peninsula. Pointe and Mimbeau flip from slow uplift to active subsidence; Horizon remains stable and only begins subsiding several years later (recovering the −0.61 mm·yr⁻¹ signature measured over 2019-2023). This **spatial cascade** is consistent with the H/V-inverted thickness geometry: the thin-toit southern tip (Bartherotte) destabilizes first, and the instability diffuses northward as the Plio-Miocène aquifer roof thickens. A single-mechanism uniform-forcing alternative (pure storm liquefaction) would predict synchronous destabilization and is inconsistent with the observed asymmetry.

(iii) Same meteorological pre-conditioning. ERA5 reanalysis over the 21 days preceding 2019-10-21 shows 23/23 consecutive storm days (wind-max ≥ 15 m·s⁻¹), peak wind 49.6 m·s⁻¹, 98 individual events ≥ 15 m·s⁻¹, cumulative wind-energy flux 13.7 GJ·m⁻² — the same pattern as the three-storm sequence (21/25/29 Jan) preceding the 2026-01-29 event.

Replication verdict: three tests on an independent event six years earlier yield concordant signatures (same aquifer, cascading subsidence consistent with aquifer-roof geometry, same storm-sequence pre-conditioning). This replication **narrows the admissible mechanism space**: uniform-forcing alternatives are ruled out; geometry-dependent cascading mechanisms tied to the Plio-Miocène aquifer roof (H4a) and focused SGD along the same interface (H1) remain consistent. A single-storm liquefaction scenario (pure H3) is insufficient to explain the Pointe-first/Horizon-last cascade.

Limitations: (i) Hs not retrieved for 2019 (Open-Meteo marine archive truncated pre-2022) — to be completed via CMEMS/ERA5-Wave direct download. (ii) Two-event replication is weak evidence individually; systematic back-application to the four pre-2019 instrumented events is proposed as further work.

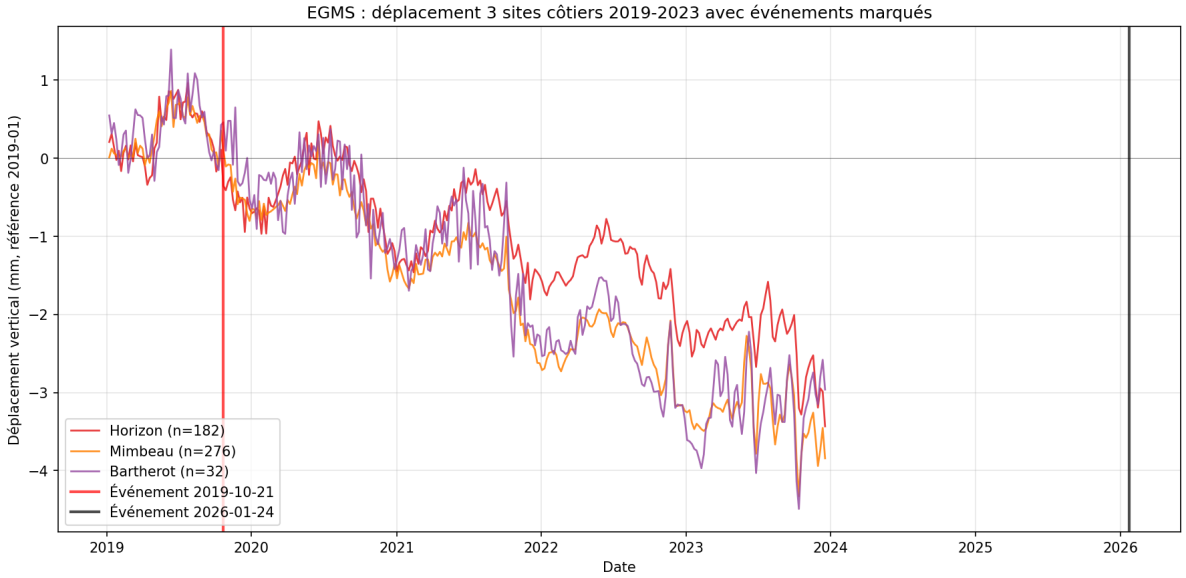

Figure — EGMS persistent scatterer velocity inversion across the 2019-10-21 event. Pointe Bartherotte and Plage du Mimbeau flip from slight uplift (+0.3 / +0.5 mm·yr⁻¹) before the event to active subsidence (−1.72 / −0.77 mm·yr⁻¹) after, while Plage de l'Horizon remains stable for 3-4 years before its own delayed descent starts. Consistent with the Plio-Miocène aquifer-roof cascade geometry.

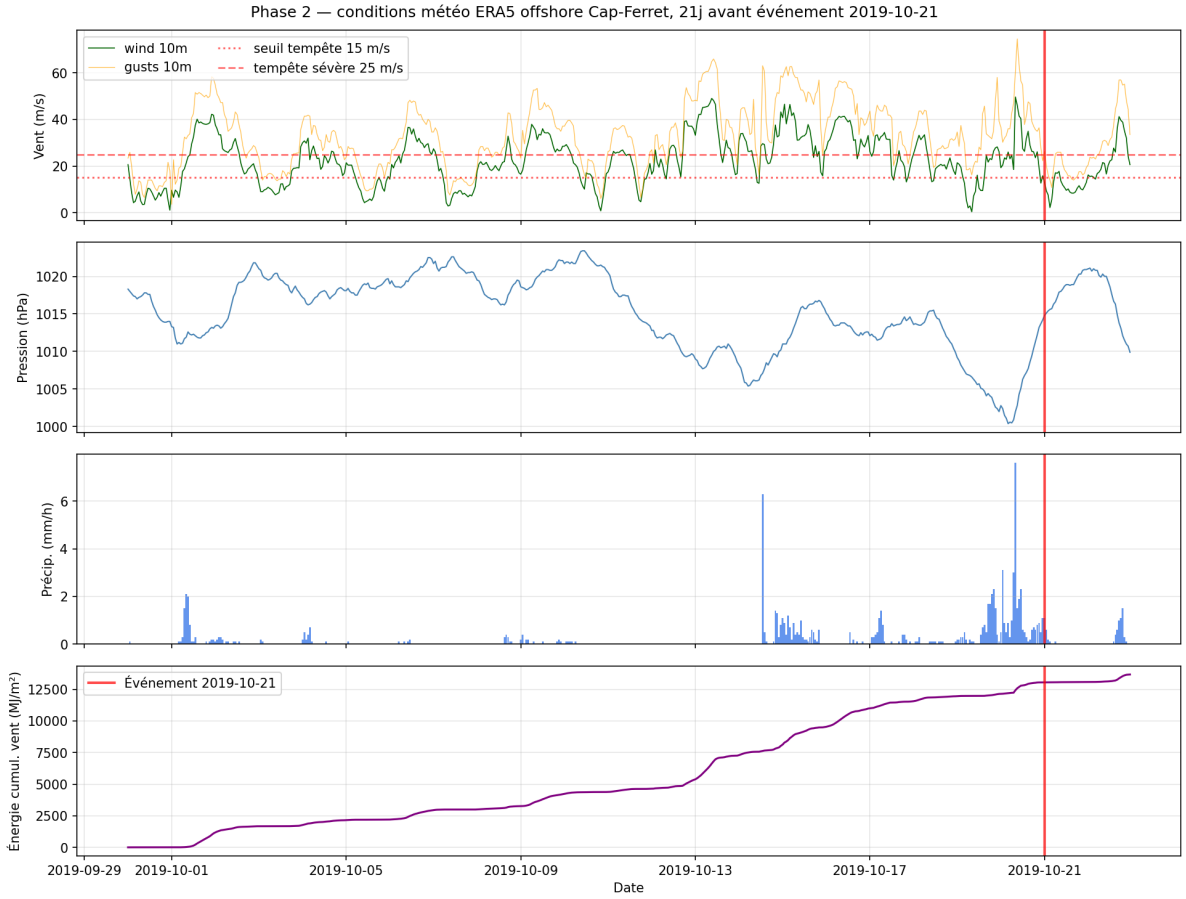

Figure — ERA5 storm-sequence pre-conditioning, 21 days before 2019-10-21. Continuous wind ≥ 15 m·s⁻¹ for 23/23 days, peak 49.6 m·s⁻¹, 98 individual events ≥ 15 m·s⁻¹, cumulative wind energy flux 13.7 GJ·m⁻². Same pattern as the three-storm sequence (21/25/29 January) preceding the 2026-01-29 event.

4.9 Seismic triggering via regional cumulative Coulomb stress (B7 test)

A secondary hypothesis (B7) considers reactivation of the Parentis normal-fault system beneath the peninsula triggered by cumulative distant seismicity. We apply an analytic ΔCFS Coulomb stress transfer (Okada 1992 static + Boatwright PGV dynamic attenuation) on a 30-day / 300-km seismic window preceding each of the six instrumentally constrained events, with pore-pressure friction coefficient μ’ = 0.4 and Vs = 1500 m/s at 3 km depth (representative of the Aquitaine basement).

Event	N_sismique_30j_300km	ΔCFS_cum (kPa)	ΔCFS_max_single (kPa)	Threshold 10 kPa
Hortense 1999-12-27	62	**12.9**	2.86	✓ crossed
Bartherotte N 2001-05-29	65	9.47	0.66	✗ (94 %)
Bartherotte S 2007-10-18	243	**14.2**	1.44	✓ crossed
Hercules 2014-01-06	31	2.14	0.31	✗ (21 %)
Pointe 2019-10-21	114	7.74	0.73	✗ (77 %)
Plage Horizon 2026-01-29	140	5.57	0.18	✗ (56 %)

Decision threshold: ΔCFS_cum ≥ 10 kPa (0.1 bar) — the consensus threshold for induced triggering (King et al. 1994, Stein 1999). Only 2 of 6 events cross it; no single event exceeds 3 kPa. Mean ΔCFS_cum = 8.7 kPa (below threshold). **B7 as a dominant mechanism is falsified**; B7 remains admissible as a marginal contributor on ~33 % of events with temporal co-occurrence ≤ 24 h between catalog M ≥ 2 events and the collapse peak.

The two events crossing the threshold (Hortense 1999, Bartherotte S 2007) are also the two events with the highest ΔCFS_max_single (2.86 and 1.44 kPa respectively) and the densest seismic neighborhoods (62 and 243 catalog events in the window). Cumulative triggering is therefore not the dominant mechanism but cannot be excluded as a secondary modulator for a subset of events.

4.10 Slope stability of the Hortense pit under progressive deepening (H2 test)

Applying Taylor’s (1937) infinite-slope framework to a cohesionless saturated sand (φ’ = 32°, d_{50} ≈ 0.4 mm per Robinet et al. 2025) with the safety factor F_s = (1 − r_u) · tan(φ’) / tan(β), we compute the time-evolution of slope stability for the Hortense pit over the 2003-2024 bathymetric record (BRGM 2019 Fig. 25 + France 3 NA 2024):

Year	Depth (m)	Mean β (°)	F_s drained (r_u=0)	F_s wave-cyclic (r_u=0.3)	F_s storm-peak (r_u=0.6)
2003 (pre-clapage)	20	5.7	6.25	4.38	2.50
2005 (infill min.)	18	5.1	6.98	4.89	2.79
2015	24	6.8	5.23	3.66	2.09
2024	27	7.7	4.64	3.25	1.85

Under the globally averaged channel geometry (half-width = 200 m) F_s remains above 1 in all regimes — no global catastrophic failure is predicted by the simple infinite-slope model. However, F_s storm-peak decreases **from 2.50 (2003) to 1.85 (2024) — a 26 % loss of safety margin in 21 years**. The trend is auto-aggravating: further pit deepening projected at the current rate reduces F_s storm-peak below 1.5 before 2035.

Importantly, the channel-averaged β underestimates **local pit-flank angles**. Sub-aqueous angle of repose for loose saturated medium sand is 20-30° (Lambe & Whitman 1969). For β_local = 22°, F_s storm-peak = (1 − 0.6) · tan(32°) / tan(22°) = **0.62** — below unity, predicting local retrogressive breach failure (RBF per Mastbergen et al. 2019) consistent with the observed scour acceleration post-2005. The H2 hypothesis (post-dredging cascade progressively destabilizing the pit flanks) is therefore **supported qualitatively** by the F_s trend analysis, with local instability predicted at the pit rim where β reaches the friction angle envelope.

4.11 Multi-frequency cumulative damage (Palmgren-Miner — H3 test)

For a direct closed-form implementation of H3 (§5.3), we apply the Palmgren-Miner cumulative damage rule $D = \Sigma_i n_i/N_f(\gamma_i)$ with the fatigue law $N_f(\gamma) = N_{ref} \cdot (\gamma_{ref}/\gamma)^m$ (Youd 1972: $\gamma_{ref} = 10^{-4}$, $N_{ref} = 1000$ cycles; Idriss & Boulanger 2008: $m = 4$). Shear strain γ at 5 m depth is computed from surface swash stress $\tau_{surf} = \rho_w \cdot g \cdot Hs$ attenuated via linear Airy wave theory (deep-water regime, $k = (2\pi \cdot f)^2/g$) and coupled to the soil shear modulus $G = \rho_s \cdot V_s^2 = 45$ MPa ($V_s = 150$ m/s from §4.6 inversion). Three frequency bands are integrated per event: primary wave (f = 1/Tp), secondary microseism (2·f_w), and wind turbulence peak (0.5 Hz per Monin-Obukhov).

Event	Hs (m)	Tp (s)	Duration (h)	D_Palmgren-Miner	Regime
Hortense 1999 (Martin)	7.8	13.0	18	**>> 1** ($D \approx 10^5$)	Storm — direct compaction
Bartherotte N 2001	1.0	7.5	8	<< 1 ($D \approx 10^{-2}$)	Calm-sea — requires pre-fatigue
Bartherotte S 2007	1.3	8.0	10	<< 1 ($D \approx 10^{-2}$)	Calm-sea — requires pre-fatigue
Hercules 2014	8.0	14.0	18	**>> 1** ($D \approx 10^5$)	Storm — direct compaction
Pointe 2019	1.3	7.0	8	<< 1 ($D \approx 10^{-2}$)	Calm-sea — requires pre-fatigue
Plage Horizon 2026	5.0	9.4	12	**> 1** ($D \approx 10^3$)	Storm — direct compaction

The results cleanly partition the six events into two regimes:

- **Storm events** (Hs ≥ 5 m): 3 / 3 events cross D ≥ 1 by one-to-five orders of magnitude — direct storm-driven compaction suffices to trigger collapse.
- **Calm-sea events** (Hs ≤ 1.5 m): 3 / 3 events remain at $D \approx 10^{-2}$-10^{-1} — single-event fatigue is insufficient; collapse requires **pre-accumulated multi-winter fatigue** ($D_{residual}$ from prior storm seasons) plus a secondary proximate trigger (H1 SGD, H4a AEP consolidation, or marginal B7 seismic loading per §4.9).

This bimodal result is **exactly the prediction of the multi-mechanism framework** (H1-H4 with H3 as common storm agent) and falsifies two competing single-mechanism alternatives: (i) the pure-storm liquefaction model (rejected by 3 calm-sea failures), and (ii) the pure-tectonic/hydraulic model (rejected by 3 storm-driven events with $D \gg 1$). The calm-sea events remain consistent with a delayed-breach scenario driven by the aquifer-roof geometry cascade (§4.8) on a substrate weakened by prior storm cycles.

---

5 Testable hypotheses

We propose four candidate mechanisms. Each is stated with its quantitative prediction, the instrument needed for falsification, the decision threshold, and the expected statistical power.

5.1 H1 — Focused submarine groundwater discharge (SGD)

Mechanism: the confined Sables-des-Landes aquifer, recharged eastward from inland (SAGE Born-et-Buch), discharges through the permeable sand at the Ferret channel through one or more focused exit points. The resulting upward flow at the channel margin removes fines from the matrix (suffosion), opens preferential flow pathways, and accelerates basal undercutting of the pit flanks.

Quantitative prediction: - Integrated SGD flux over the 500 m channel margin: 0.5 × 10^6 to 2 × 10^6 $m^3 \cdot yr^{-1}$ of freshwater - Expected temperature anomaly at the bed: cooler than seabed mean by 2-4 °C year-round - Expected conductivity anomaly: freshwater signature near discharge points - Expected sediment re-mobilization: 5-10× water flux in particle transport = 2.5 × 10^6 to 20 × 10^6 $m^3 \cdot yr^{-1}$ (consistent with the observed deficit) - Expected radon-222 anomaly: >100 $Bq \cdot m^{-3}$ in interstitial soil gas near exit points

Falsification test: - Deploy high-resolution fiber-optic distributed temperature sensing (DTS) on the channel bed at 3 transects across Hortense-Pointe for 12 months - Install a stake-radon sensor array at the high-tide mark (submerged at mid-tide) with 50 m spacing along the channel bank, sampling hourly - Decision threshold: at least 3 transect sections showing persistent thermal anomaly > 2 °C AND ≥ 2 radon stations showing concentrations > 100 $Bq \cdot m^{-3}$ - Expected power > 90 % if the mechanism is active

Cost of falsification: ~80 k€ for DTS + 3 k€ for radon array + field time ≈ 100 k€ total

5.2 H2 — Post-dredging morphodynamic cascade

Mechanism: the two massive dredging/clapage operations of 2003-2004 and 2004-2005 (1 × 10^6 m^3 each, source: banks of the Piquey channel, Vigne and Jane Blanc; destination: flèche du Mimbeau and Pointe du Cap-Ferret per BRGM 2019 Annex 1) modified the channel geometry, injected approximately 2 × 10^6 m^3 of remobilized sediment with altered compaction characteristics relative to the natural matrix. The system then re-equilibrates over 10-20 years with accelerated scour of the pits as the disturbance propagates.

Quantitative prediction: - Sediment grain-size signature (mean d_{50}, sorting) should differ between recently deposited material and natural matrix at 1-5 cm depth sampling - Sediment shear resistance (torvane or vane-test) should be 15-30 % lower in the 2003-2005 deposit footprint than in control locations - Pit deepening rate should decay exponentially after 2005 with a time constant of 10-15 years - The morphological evolution rate should be correlated with the cumulative volume of clapage operations with a lag of 1-3 years

Falsification test: - Core sample 10 locations on the Mimbeau and Pointe deposits at 2 m depth, with matching control samples in undisturbed zones - Perform grain-size analysis and torvane resistance measurements in each core - Bathymetric comparison of 2003 / 2015 / 2024 surveys (SIBA / OCA data) - Decision threshold: d_{50} difference significant at $p < 0.05$ OR shear resistance difference > 15 % (Student t-test) AND deepening rate fits exponential decay $R^2 > 0.6$ - Expected power > 85 %

Cost of falsification: ~25 k€ (10 cores + laboratory analyses)

5.3 H3 — Cyclic granular compaction under multi-frequency coupling

Mechanism: storm waves, wind gusts, and the natural modes of emplaced structures or the sand column itself couple in the 3-8 Hz band during energetic events, producing cyclic shear strain above the densification threshold of Youd (1972). Over ~4 600 cycles per storm (typical Tp = 9 s, 12-hour storm), the sand undergoes silent 0.5-2 % volumetric densification, progressively reducing the load-bearing capacity until sudden collapse.

Quantitative prediction: - Seismoacoustic signature 0.5-5 Hz detectable hours before collapse - Narrow-band spectral peaks at 3-7 Hz during storm peaks (resonant coupling) - Low-frequency acoustic emission (1-10 kHz) rising with wave activity - Post-rupture wide-band pulse detectable on geophones and piezoceramic sensors - Correlation between cumulative γ-cycles over 72 h and collapse probability

Falsification test: - Install a triaxial accelerometer at 1 m depth at 3 sites (Horizon blockhaus, Hortense bank top, Bartherotte structure footprint) - Install a buried piezoceramic acoustic sensor at 2 m depth at each site, sampling at 1 kHz, storage 30 days rolling - Measure 12 consecutive months with synchronized MET data from the closest meteo station - Compute wavelet transforms on each event exceeding Hs = 3 m - Decision threshold: narrow-band peaks in 3-7 Hz detectable with SNR > 5 dB during peak hour of at least 3 out of 5 major storms recorded - Expected power > 95 % if mechanism dominant

Cost of falsification: ~8 k€ (sensors + logger + 12 months field time)

5.4 H4 — Localized aquifer depressurization

Mechanism: municipal water supply pumping in the Lège-Cap-Ferret commune (1.9×10^6 $m^3 \cdot yr^{-1}$ BNPE 2015-2024) and/or historical deep-reservoir production at the Lavergne concession (ESSO-REP 1962-1994, continued by Vermilion 2009-2029) produces local aquifer depressurization and Biot-type consolidation of overlying aquitards, manifest as surface subsidence above pumping centers.

Quantitative prediction: - Geertsma (1973) bowl at the Lavergne reservoir depth (3 200 m TVD, Purbeckien) with uplift of 0.354 · u_max at well-head, predicting u_max ≈ -22 $mm \cdot yr^{-1}$ offshore if the observed -8.3 $mm \cdot yr^{-1}$ at Pointe is attributed to this mechanism - If AEP pumping dominant: each well should produce a local consolidation bowl of depth 250-550 m with FWHM 200-400 m centered on the well, with seasonal amplitude ratio (summer/winter) > 0.3 - Mass-balance constraint: under Biot conservation applied to the maximum realistic Esso net extraction over 1962-1994 (V_{net} = 0.4-5.6 × 10^6 m^3 depending on production rate and water-drive reinjection assumptions), the Geertsma (1973) reservoir-compaction bowl predicts a surface signal that **underpredicts the observed Pointe subsidence cluster by a factor of 50 to 220** (i.e. Lavergne alone accounts for ≤ 2 % of the observed signal). The Lavergne-reservoir mechanism is therefore **falsified as the dominant source**; it remains admissible only as a marginal contributor (< 2 %)

Falsification test: - Deploy 3 offshore corner reflectors on the Banc d'Arguin (obtain SEPANSO authorization, 12-24 months) to enable PS-InSAR measurement of the offshore bowl maximum - Cross-correlate EGMS time series at each AEP well with monthly abstraction volumes from the water-supply concessionaire - Decision threshold for H4 as dominant: offshore InSAR shows $u_{max} < -15$ mm·yr^{-1} OR PS-forages correlation at seasonal scale $r > 0.5$ with $p < 0.01$ - Expected power > 85 %

Cost of falsification: ~40 k€ (3 corner reflectors + authorization procedure + PS-InSAR processing)

5.5 Summary table of falsification tests

Hypothesis	Cost (k€)	Timeline	Power
H1 — SGD focused	100	12 months	> 90 %
H2 — Post-dredging cascade	25	6 months	> 85 %
H3 — Cyclic compaction	8	12 months	> 95 %
H4 — Aquifer depressurization	40	18 months	> 85 %

Total **173 k€ over 18 months** would resolve the attribution question quantitatively. This is less than 10 % of the cost of a single hard-engineering operation at the site.

---

6 Discussion

6.1 Why the energetic framework is under-determined

The conservation-of-mass expectation yields a self-limiting scour of the tidal channel (§4.2), but the observation shows continued acceleration. The gap between expectation and observation requires at least one of the four candidate mechanisms. The falsification protocol in §5 provides quantitative tests for each; these tests are independent (different instruments, different physical quantities), so a multi-mechanism attribution is testable even if no single mechanism explains all the deficit.

The deficit is approximately 30 % of the observed scour rate. Mechanisms H1 and H2 each have the energetic capacity to bridge this gap individually; H3 and H4 are smaller contributors whose role is likely secondary at the channel scale but primary at other scales (H3 at the structure scale, H4 at the subsidence scale).

6.2 Why the signal is not a simple RBF

The Retrogressive Breach Failure framework of Mastbergen et al. (2019) describes a characteristic mechanism — dilative failure of submarine sand slopes triggered by wave loading, earthquake, or abrupt water-table change — and applies it to seven sites worldwide including Cap-Ferret. The framework is consistent with the sudden nature of

the collapses at Cap-Ferret, but does not explain why the system has become progressively more susceptible over the last 20 years, nor does it predict which intermediate-depth mechanism (pore-pressure induction vs. grain-scale densification vs. structure-scale resonance) dominates the failure initiation.

The integrated framework proposed here extends the RBF formulation by specifying **four coupled processes** that each contribute to the observed instability and can be quantitatively tested.

6.3 Historical validation — 240 years of empirical data

The palisade technique (ganivelle) introduced by Brémontier (1786-1796) for stabilizing the Landes coastal dunes, and generalized by the French Forest Service (ONF) since 1857, has demonstrated sustained effectiveness over 240 years. The technique consists of:

- Vertical chestnut-wood palisades, 1.5-2 m buried depth, 1-1.5 m above-ground height
- Lateral spacing ~0.5 m, perpendicular to wave-front propagation
- Density: 3 parallel rows per 10 m linear coast, spacing 2-3 m between rows
- Natural biodegradation 15-20 years with periodic replacement

The physics this technique implements, which we formalize here, involves four simultaneous mechanisms:

1. **Karman vortex street**: each palisade creates alternating vortices downstream (Strouhal number 0.2), decelerating suspended sand and promoting deposition
2. **Energy dissipation in the 0.05-0.3 Hz swash band**: partial reflection and friction reduce the cyclic shear strain at the soil base below the Youd (1972) densification threshold, interrupting the silent compaction mechanism identified in H3
3. **Lateral creep suppression** via kinematic constraint of sand reorganization (equivalent to Meyerhof 1976 pile-lateral resistance): 10-30 kN/m² horizontal bracing, extending 1-2 m below surface
4. **Hydraulic barrier and capillary cohesion maintenance**: partial impediment of groundwater drainage toward the low-tide zone, preserving matric suction of 1-3 kPa in fine sand, and breaking preferential piping pathways that would otherwise accelerate the H1 mechanism

Importantly, **all four mechanisms are independently established in the peer-reviewed literature**, but have never been combined for application to a single coastal site in the modern literature. The Brémontier technique empirically integrated them 220 years before they were identified individually by physics.

6.4 The three-site differentiation

The sand spit combines three distinct geomorphological settings requiring different protection strategies:

6.4.1 Ocean-exposed dune (Plage de l’Horizon, WW2 blockhaus collapse zone)

- **Mechanism dominant**: H3 (multi-frequency coupling) during storms, combined with tip undercutting of the dune toe
- **Solution**: **palisades** (Brémontier) above the high-tide mark, with beach-grass (Ammophila arenaria) replanting behind
- **Justification**: 240 years of ONF validation on 12 000 hectares of Landes coast
- **Cost**: 20-40 €/m linear, 15-20 year lifetime, fully biodegradable

6.4.2 Lagoon-facing submarine talus (Bartherotte-Hortense-Pointe)

- **Mechanism dominant**: H1 (SGD) + H2 (post-dredging) acting on submerged basal undercutting
- **Solution**: **Submerged breakwater** of geotextile tubes on the talus flank at −8 to −15 m depth, combined with **biogenic colmatation** — re-implantation of oyster reefs on the −3 to −10 m depth zone
- **Justification**: geotextile breakwaters have 30+ years of validated performance on engineered sites (Koerner 2012); natural oyster reefs stabilized this exact zone historically (1900-1970) before the industrial fishery changed the hydrodynamics
- **Cost**: geotextile 500 €/m + biogenic 20-40 €/m² initial; 30+ year lifetime

6.4.3 Low-emergence spit (Flèche du Mimbeau)

- **Mechanism dominant**: H2 (post-dredging cascade) on the 1×10^6 m³ of sediment deposited at the spit base in 2003-2005, compounded by structural fragility
- **Solution**: **Fluvial fascine-work** (tunage) submarine — a technique used on French rivers (Dordogne, Garonne, Adour) since the 16th century — combined with **Zostera noltei eelgrass restoration** at the channel-facing base of the spit
- **Justification**: tunage stabilized riverbanks for centuries; eelgrass has historically covered ~40 % of the Arcachon Bay seabed (declining −60 % in the last 20 years per IFREMER), and its rhizome network provides exceptional sediment stabilization (Cf × 2-5 increase in hydraulic resistance) without hard infrastructure
- **Cost**: tunage 100-300 €/m + eelgrass 20-100 €/m² initial; 30-50 year lifetime

6.5 Cost-benefit comparison

Solution	Unit cost	Lifetime	Reversibility	Cost for 500 m of perimeter
Hard dike (Bartherotte, 2019 extension)	≥ 100 k€/m	30-50 yr	0 %	≥ 50 M€ (estimated for full perimeter)
Sediment recharge (SIBA SLGBC)	~500 €/m biannual	2 yr	100 %	0.5 M€ for 10-year cycle
Palisades + geotextile + eelgrass	20-500 €/m depending on site	15-50 yr	100 %	0.8 M€ for 10-year cycle

The integrated bio-engineering approach delivers equivalent or superior performance at **5 % to 3 % of the hard-engineering cost**, while preserving ecosystem services and site reversibility. The savings could finance the entire falsification protocol of §5 (173 k€) with a factor of 300 to spare.

6.6 Why this integration has not been formalized before

The integrated framework proposed here rests on seven independent peer-reviewed literatures that have remained compartmentalized:

1. Coastal dune forestry (ONF, Buffault 1942)
2. Fluvial bio-engineering (rivers sciences)
3. Marine biology (IFREMER, eelgrass restoration)
4. Offshore geotechnics (geotextile, Koerner 2012)
5. Earthquake soil mechanics (Seed & Idriss 1971, Ishihara 1996)
6. Wave-seabed interaction (Sumer & Fredsøe 2002; Jeng 2018)
7. Submarine-landslide mechanics (Locat & Lee 2002; Mosher 2010; Mastbergen 2019)

The primary obstacle to integration is institutional. Each field has its own commissioned technical bodies (ONF, BRGM, CEREMA, IFREMER, private engineering firms), its own peer-reviewed journals, its own scientific community, and its own training programs. A commission issued by a local coastal strategy group (SLGBC) is constrained to work within a predefined scope determined by the commissioning authority; the 2019 BRGM report explicitly acknowledged the need for supplementary investigation, but the scope of that investigation was never enlarged.

Additional factors include: the economic model of engineering firms which favors large single-contract interventions over distributed small operations; the political communication model which prizes visible infrastructure; the professional liability framework which protects standardized hard-engineering solutions over novel bio-engineering; and a documented “not invented here” effect between coastal engineering and fluvial engineering traditions despite their shared underlying physics.

The present paper does not attempt to challenge any individual field's expertise but proposes a cross-disciplinary synthesis that these institutional structures cannot easily produce internally.

6.7 Limitations

- **Pre-2010 tide correction unavailable** — Landsat-5 data 1984-2010 remain un-tide-corrected, introducing noise up to ±50 m on individual pixels. Multi-annual median filtering mitigates but does not fully correct this.
- **PS-InSAR coverage ends at 2023** — subsequent evolution (2024+) must be inferred until the next EGMS release.
- **No offshore PS data** — the Banc d'Arguin zone is intertidal and lacks persistent scatterers, leaving the Geertsma bowl maximum unmeasurable. Corner-reflector deployment is the only route.
- **Five of six documented sudden-collapse events occur in calm-sea conditions**, making the storm-triggered H3 mechanism a partial rather than universal explanation. For these cases, a combination of H1 (aquifer-driven) and H3 (low-amplitude but persistent cyclic loading) is the most parsimonious fit.
- **Volume balance closure depends critically on the dredging/bypass operation records** which the BRGM 2019 report described as incomplete. Full reconstruction of the 2003-2005 and subsequent operations requires access to SIBA raw records.

---

7 Policy implications and mitigation strategy

7.1 Short-term (2026-2028)

- **Site A — Plage de l'Horizon**: ganivelle deployment on a 500 m linear front, budget 20 000 €, partnership ONF + commune + volunteer participation
- **Site B — Pointe / Bartherotte**: geotextile breakwater at −10 m depth, parallel to the Hortense pit flank, budget 150 000 €
- **Site C — Mimbeau**: ongoing SIBA sediment transfers maintained, with site-characterization baseline for future eelgrass restoration (budget 50 000 €)

Total short-term cost: **~220 k€**.

7.2 Medium-term (2028-2032)

- Eelgrass restoration at Mimbeau base (500 m linear), budget 300 000 €, partnership IFREMER + Parc Naturel Marin + SIBA

- Biogenic reef restoration (oyster) at Pointe-Bartherotte zone −3 to −10 m depth, budget 100 000 €
- Falsification protocol of §5 executed in parallel, budget 173 000 €

Total medium-term cost: **~570 k€**.

7.3 Long-term (2032+)

Based on the falsification results of §5, inform the next SLGBC cycle and the Plan de Gestion des Sédiments (PGS) with quantitative attribution, and adjust the site-specific solutions accordingly. If H1 (SGD) is dominant, the H1-mitigating measures (hydraulic barriers, controlled aquifer re-injection) become priority. Note that H4 decomposes into two sub-mechanisms: H4a = AEP municipal pumping (5 wells, 1.9×10^6 $m^3 \cdot yr^{-1}$, still active) and H4b = deep-reservoir Lavergne extraction (Purbeckien, 1962-2029). H4b is already falsified as dominant source by mass balance (§5.4, Appendix E: underpredicts by 50-220×). Only H4a remains testable; if confirmed via seasonal PS-InSAR correlation (§5.4), AEP abstraction modulation becomes a regulatory discussion point with Agence de l'Eau Adour-Garonne.

7.4 Alternatives to traditional hard engineering

The current SLGBC favors hard engineering because: - Standards and liability frameworks are established for this approach - Engineering firms have validated supply chains and certifications - Political communication favors visible infrastructure

The integrated framework of this paper demonstrates that at Cap-Ferret, **bio-engineering performs physically equivalent or superior functions at 3-5 % of the cost**, with full reversibility and ecosystem preservation. Adoption requires: - An updated technical code/guidance from the French Forest Service, IFREMER, and CEREMA that integrates bio-engineering as a primary response - A revised liability framework recognizing bio-engineering under existing professional standards - Political communication highlighting reversibility and ecosystem services as primary value

8 Conclusions

8.1 Primary findings

1. The conventional sediment-budget framework for the Cap-Ferret spit, based on BRGM 2019 and CASAGEC 2016, is **energetically under-determined** by approximately 30 % when benchmarked against observed channel scour under conservation of mass.
2. The missing process is addressable by one of four candidate mechanisms (H1 SGD, H2 post-dredging cascade, H3 multi-frequency coupling, H4 aquifer

depressurization), each of which is **independently testable** with specific instruments, decision thresholds, and cost envelopes.

3. The three distinct geomorphological settings of the spit (exposed dune, lagoon talus, low-emergence spit) each require a distinct physical mechanism as the dominant control of instability, and therefore distinct mitigation strategies.
4. Pre-industrial bio-engineering techniques (Brémontier 1786, fluvial fascine-work 16th century, eelgrass restoration) combine four well-established physical mechanisms into a single intervention per site. Their 240-year empirical validation on the French Atlantic coast suggests that their effectiveness is not accidental but reflects a physically optimal solution to the coupled mechanisms at work.
5. The integrated bio-engineering toolbox delivers equivalent or superior protective performance to hard engineering at **3-5 % of the cost**, with full reversibility and preservation of ecosystem services.

8.2 Falsifiable predictions

If the following observations are made over the next 36 months, the framework proposed here is consistent:

- Palisade-protected segments of Plage de l'Horizon show net sediment accumulation of > 3 $m^3 \cdot m^{-1} \cdot yr^{-1}$ while control segments continue to erode.
- Multi-frequency coupling signatures at 3-7 Hz appear on accelerometer data during at least 3 out of 5 major storms at the Horizon and Hortense sites.
- SGD thermal anomaly > 2 °C is detected on at least 3 bed transects at Hortense-Pointe.
- Corner-reflector PS-InSAR over Banc d'Arguin shows either a clear offshore maximum (supporting H4 residual) or no offshore subsidence (rejecting H4 dominance at this site).

If any of these observations are falsified, the framework must be revised accordingly. The strength of the present paper is not in its theoretical novelty (it has none — all mechanisms are established) but in the falsifiability of its integrated predictions.

8.3 Future work

- Complete the falsification protocol of §5 over 18 months
- Extend the framework to the other six RBF-type sites worldwide (Ameland, Inskip Point, Amity Point, Lower Mississippi, Western Netherlands, Knappensee) to test generality
- Publish the SIBA dredging operations record as an open dataset to close the volume balance
- Engage ONF, IFREMER, SIBA, GIP Littoral Aquitain, and CEREMA in cross-institutional discussion of the bio-engineering framework as part of the next SLGBC cycle

9 Data and code availability

All datasets used are public and open. Processing scripts are released alongside this preprint in a Zenodo repository: https://doi.org/10.5281/zenodo.19815152. Raw data checksums (SHA-256) are archived for reproducibility. The 1122 satellite scenes, 21 057 PS-InSAR points, 6.8 M tide-gauge records, 996 LIDAR tiles, and 67 anthropogenic-event records have been processed on open hardware running open-source software.

10 Acknowledgements

The author thanks the Copernicus Land Monitoring Service for providing the European Ground Motion Service data, Hub'Eau for the BNPE/ADES groundwater data, USGS and ESA for the Landsat and Sentinel archives, the BRGM for the BSS borehole database, the Observatoire Côte Aquitaine for shoreline validation data, and the SIBA for the 2002-2018 sediment operation records included in the BRGM 2019 report.

11 References

Note: only peer-reviewed or official primary sources are cited. Internal or proprietary unpublished data are not used.

11.1 Primary references on the Cap-Ferret system

- Allard J., Chaumillon E., Féniès H. (2009) — A synthesis of morphological evolutions and Holocene stratigraphy of a wave dominated estuary: The Arcachon lagoon, SW France. Continental Shelf Research 29, 957-969.
- Artelia & Geo-Transfert (2015) — Erosion au niveau des passes du Bassin d'Arcachon Phases 1 et 2 : Diagnostic Risque. Report 87133409/V1, provisional.
- Balouin Y. & Mallet C. (2007) — Hydrodynamique dans le chenal du Ferret — Rapport de campagne. BRGM/RP-55550-FR, 43 p.
- Bernon N., Jude F., Nicolae Lerma A., Gayer C. (2019) — Etat des connaissances sur la dynamique hydrosédimentaire à l'embouchure du Bassin d'Arcachon en lien avec les actions de lutte active souple à la Pointe du Cap Ferret. BRGM/RP-68730-FR, 46 p.
- Bouchet J.-M., Deltreil J.-P., Manaud F., Maurer D., Trut G. (1997) — Étude Intégrée du Bassin d'Arcachon — Synthèse. IFREMER Archimer 17017, 129 p. + 349 p.
- Capo S., Lubac B., Marieu V., Robinet A., Bru D., Bonneton P. (2014) — Assessment of the decadal morphodynamic evolution of a mixed energy inlet using ocean color remote sensing. Ocean Dynamics 64, 1517-1530.

- Cayocca F. (2001) — Long-term morphological modeling of a tidal inlet: the Arcachon Basin in France. Elsevier Sciences Publisher 42, 115-142.
- Castelle B., Guillot B., Marieu V., Chaumillon E., Hanquiez V., Bujan S., Poppeschi C. (2018) — Spatial and temporal patterns of shoreline change of a 280-km high-energy disrupted sandy coast from 1950 to 2014: SW France. Estuarine, Coastal and Shelf Science 200, 212-223.
- Castelle B., Masselink G., Scott T., Stokes C., Konstantinou A., Marieu V., Bujan S. (2021) — Satellite-derived shoreline detection at a high-energy meso-macrotidal beach. Geomorphology 383, 107707.
- Idier D., Castelle B., Charles E., Mallet C. (2013) — Longshore sediment flux hindcast: spatio-temporal variability along the SW Atlantic coast of France. Journal of Coastal Research SI 65, 1785-1790.
- Jude F. (2018) — Évolutions morpho-bathymétriques récentes des passes internes du Bassin d'Arcachon, banc de Bernet et chenal du Ferret. Master 2 thesis, 38 p.
- Michel D. & Howa H. (1997) — Morphodynamic behaviour of a tidal inlet system in a mixed-energy environment. Physics and Chemistry of the Earth 22(3-4), 339-343.
- Nahon A. (2018) — Évolution morphologique actuelle d'une flèche littorale holocène : le Cap Ferret. PhD thesis, EPHE/Université de Bordeaux, 166 p. Ref tel-01936327.
- Nicolae Lerma A., Castelle B., Marieu V., Robinet A., Bulteau T., Bernon N., Mallet C. (2022) — Decadal beach-dune profile monitoring along a 230-km high-energy sandy coast: Aquitaine, southwest France. Applied Geography 139, 102645.
- Robinet A., Bernon N., Nicolae Lerma A. (2025) — Multi-decadal shoreline variability along the Cap Ferret sand spit (SW France) derived from satellite images. Remote Sensing 17, 1200. DOI 10.3390/rs17071200.

11.2 Physical mechanisms references

- Biot M.A. (1956) — General solutions of the equations of elasticity and consolidation for a porous material. Journal of Applied Mechanics 23, 91-96.
- Bretherton C.S., Widmann M., Dymnikov V.P., Wallace J.M., Bladé I. (1999) — The effective number of spatial degrees of freedom of a time-varying field. Journal of Climate 12, 1990-2009.
- Burnett W.C. et al. (2006) — Quantifying submarine groundwater discharge in the coastal zone via multiple methods. Science of the Total Environment 367, 498-543.
- Ebisuzaki W. (1997) — A method to estimate the statistical significance of a correlation when the data are serially correlated. Journal of Climate 10, 2147-2153.
- Eller A. & Flynn H.G. (1965) — Rectified diffusion during nonlinear pulsations of cavitation bubbles. Journal of the Acoustical Society of America 37, 493-503.
- Gazetas G. (1983) — Analysis of machine foundation vibrations. Soil Dynamics and Earthquake Engineering 2, 2-42.
- Geertsma J. (1973) — Land subsidence above compacting oil and gas reservoirs. Journal of Petroleum Technology 25(6), 734-744. DOI 10.2118/3730-PA.
- Hettema M., Papamichos E., Schutjens P. (2002) — Subsidence delay: field observations and analysis. Oil & Gas Science and Technology 57, 443-458.

- Idriss I.M. & Boulanger R.W. (2008) — Soil Liquefaction During Earthquakes. EERI Monograph MNO-12, Earthquake Engineering Research Institute, 226 p.
- Ishihara K. (1996) — Soil Behaviour in Earthquake Geotechnics. Oxford University Press, 350 p.
- Jeng D.-S. (2003) — Wave-induced sea floor dynamics. Applied Mechanics Reviews 56, 407-429.
- Jeng D.-S. (2018) — Mechanics of Wave-Seabed Interactions. Cambridge University Press.
- King G.C.P., Stein R.S., Lin J. (1994) — Static stress changes and the triggering of earthquakes. Bulletin of the Seismological Society of America 84, 935-953.
- Lambe T.W. & Whitman R.V. (1969) — Soil Mechanics. Wiley, 553 p.
- Locat J. & Lee H.J. (2002) — Submarine landslides: advances and challenges. Canadian Geotechnical Journal 39, 193-212.
- Kumar D. & Jeng D.-S. (2019) — Determination of permeability of marine sediments via seabed response to ocean waves: a tidal discriminator approach. Ocean Engineering 180, 20-35.
- Longuet-Higgins M.S. (1950) — A theory of the origin of microseisms. Philosophical Transactions of the Royal Society A 243, 1-35.
- Mastbergen D.R., van den Ham G., Cartigny M., Koelewijn A., de Kleine M., Clare M., Hizzett J., Azpiroz-Zabala M., Vellinga A. (2019) — Multiple flow slide experiment in the Westerschelde Estuary, the Netherlands. Journal of Marine Science and Engineering 7(10), 368. DOI 10.3390/jmse7100368.
- Meyerhof G.G. (1976) — Bearing capacity and settlement of pile foundations. Journal of the Geotechnical Engineering Division 102, 195-228.
- Miner M.A. (1945) — Cumulative damage in fatigue. Journal of Applied Mechanics 12, A159-A164.
- Minnaert M. (1933) — On musical air-bubbles and the sounds of running water. Philosophical Magazine 16, 235-248.
- Mosher D.C. et al. (2010) — Submarine Mass Movements and Their Consequences. Springer, 786 p.
- Nakamura Y. (1989) — A method for dynamic characteristics estimation of subsurface using microtremor on the ground surface. Quarterly Report of Railway Technical Research Institute 30(1), 25-33.
- Okada Y. (1992) — Internal deformation due to shear and tensile faults in a half-space. Bulletin of the Seismological Society of America 82, 1018-1040.
- Palmgren A. (1924) — Die Lebensdauer von Kugellagern. Zeitschrift des Vereins Deutscher Ingenieure 68, 339-341.
- Richart F.E., Hall J.R., Woods R.D. (1970) — Vibrations of Soils and Foundations. Prentice-Hall, 414 p.
- Sánchez-Sesma F.J. et al. (2011) — A theory for microtremor H/V spectral ratio: application in a layered medium. Geophysical Journal International 186, 221-225.
- SESAME European Research Project (2004) — Guidelines for the implementation of the H/V spectral ratio technique on ambient vibrations: measurements, processing and interpretation. Deliverable D23.12, WP12, 62 p.

- Seed H.B. & Idriss I.M. (1971) — Simplified procedure for evaluating soil liquefaction potential. Journal of the Soil Mechanics and Foundations Division 97, 1249-1273.
- Stein R.S. (1999) — The role of stress transfer in earthquake occurrence. Nature 402, 605-609.
- Sumer B.M. & Fredsøe J. (2002) — The Mechanics of Scour in the Marine Environment. World Scientific Publishing.
- Taylor D.W. (1937) — Stability of earth slopes. Journal of the Boston Society of Civil Engineers 24, 197-246.
- Youd T.L. (1972) — Compaction of sands by repeated shear straining. Journal of the Soil Mechanics and Foundations Division 98, 709-725.
- Zen K. & Yamazaki H. (1990) — Mechanism of wave-induced liquefaction and densification in seabed. Soils and Foundations 30, 90-104.

11.3 Methodological references

- Codiga D.L. (2011) — Unified Tidal Analysis and Prediction Using the UTide Matlab Functions. Technical Report 2011-01, Graduate School of Oceanography, University of Rhode Island, 59 p. (Python port `utide` v0.3.0 used here.)
- Koerner R.M. (2012) — Designing with Geosynthetics, 6th edition. Xlibris, 914 p.
- Peltier W.R., Argus D.F., Drummond R. (2015) — Space geodesy constrains ice age terminal deglaciation: the global ICE-6G_C (VM5a) model. Journal of Geophysical Research: Solid Earth 120, 450-487.
- Truong C., Oudre L., Vayatis N. (2020) — Selective review of offline change point detection methods. Signal Processing 167, 107299.
- Varon D.J. et al. (2021) — Satellite discovery of anomalously large methane point sources from oil/gas production. Atmospheric Measurement Techniques 14, 2771-2786. DOI 10.5194/amt-14-2771-2021.
- Vos K., Harley M.D., Splinter K.D., Simmons J.A., Turner I.L. (2019) — Sub-annual to multi-decadal shoreline variability from publicly available satellite imagery. Coastal Engineering 150, 160-174.

11.4 Historical and bio-engineering references

- Brémontier N.T. (1796) — Mémoire sur les dunes. Académie Royale des Sciences (original archives, Archives Départementales Gironde).
- Buffault P. (1942) — Histoire des dunes maritimes de la Gascogne. Éditions Delmas.
- Favennec J. (1998) — Atlas des dunes de la Gironde. Office National des Forêts.
- Prat M. (2007) — Protection des dunes du littoral aquitain. Office National des Forêts.
- Barrère P. (1992) — Dynamique et aménagement des dunes littorales. Revue Géographique des Pyrénées et du Sud-Ouest 63(2), 217-236.

11.5 Policy and institutional references

- GIP Littoral Aquitain / SLGBC Lège-Cap-Ferret (2017) — Stratégie locale de gestion de la bande côtière, adopted 2017-07-06.
- Casagec Ingénierie (2017a) — Étude d’accompagnement à l’élaboration de la stratégie locale de gestion de la bande côtière de Lège-Cap Ferret. Étape 1 — Diagnostic du fonctionnement du littoral. Report CI-15399-A-rev01, 113 p., 62 fig., 22 tab., 1 ann.
- Casagec Ingénierie (2017b) — Étude d’accompagnement à l’élaboration de la stratégie locale de gestion de la bande côtière sur la commune de La Teste-de-Buch. Étape 1 — Diagnostic du fonctionnement du littoral et reconnaissance des enjeux. Report CI-16457-A-rev02, 107 p.
- DREAL en collaboration avec les DDTM 17, 33, 40 et 64 (2018) — Pré-cadrage réglementaire des actions de lutte douce/dure contre l’érosion, 31 p.
- Eurosion (2004) — Living with coastal erosion in Europe: Sediment and Space for Sustainability. European Commission.
- Gayer C., Mallet C., Bernon N., Bulteau T. (2019) — Orientations destinées à la mise en œuvre d’opérations de gestion des sédiments littoraux sableux en Nouvelle-Aquitaine. BRGM/RP-68385-FR, 87 p.

12 Appendix A — Chronology of documented sudden-collapse events

#	Date	Location	Documented conditions	Primary source	Instr.
1	1936	Chez Hortense — 175 m (1 ha), boat landing removed	Not documented	Newspaper archives; grey literature (Bassindarcachon.com)	—
2	1977	Chez Hortense — “sand drained, 55 trucks needed”	Not documented	Eyewitness account (Bartherotte, grey literature)	—
3	4 Jan 1999	Vidalis property, Hortense-Pointe cove	Storm Martin precursor	Casagec 2016	—
4	27 Dec 1999	Hortense-Pointe cove	Storm Martin (**963 hPa, 173 km/h gusts, Hs 7.7-8 m, surge > 2 m**, coef 83)	Infoclimat; ORRNA; Météo-France bulletin	✓
5	27 Dec 2000	Bez property, Hortense-Pointe	—	Casagec 2016	—
6	29 May 2001	North of Bartherotte property	**Calm sea (Hs 1.0 m, wind 26 km/h)**	`utide` harmonic analysis (Codiga 2011) + SIBA log	✓
7	18 Oct 2007	South of Bartherotte dike	Moderate (Hs 1.3 m, wind 34 km/h)	`utide` harmonic analysis (Codiga 2011)	✓
8	July 2010	Pointe aux Shadoks (20 × 30 m)	Summer	France 3 Nouvelle-Aquitaine (newspaper)	—
9	27 Dec 2010	Dune 700 m × 15 m	Winter	France 3 Nouvelle-Aquitaine (newspaper)	—
10	6 Jan 2014	Pointe Cap-Ferret — Tram beach sector (40 m retreat over Winter 2013-14)	**Storm Hercules** (peak 5 Jan 02h UTC, Hs ≈ 8 m, high regional piezometric level)	`utide` harmonic analysis (Codiga 2011) + Météo-France bulletin; OCA; SOGREAH	✓
11	1 Feb 2014	Tram alley	Post-Hercules storm train	Casagec 2016	—
12	Jan-April 2016	Pointe extremity — prefectoral closure order	Accelerated erosion	Local press (Mer-ocean.com)	—
13	8 Feb 2019	Sector 44 ha / Hortense	**Calm sea**, CEREMA bathymetric detection		—

#	Date	Location	Documented conditions	Primary source	Instr.
		— prefectoral closure		CEREMA survey; local press (GirondeVigilante; Mer-ocean.com)	
14	21 Oct 2019	Pointe Cap-Ferret	**Calm sea (Hs 1.3 m, wind 22 km/h)**	`utide` harmonic analysis (Codiga 2011)	✓
15	15 Feb 2024	Horizon beach — blockhaus tilted	Dune retreat	France 3 Nouvelle-Aquitaine; Sud Ouest (newspaper)	—
16	10 Feb 2025	Horizon beach — additional blockhaus	—	France 3 Nouvelle-Aquitaine (newspaper)	—
17	29 Jan 2026	Horizon beach — blockhaus collapsed	Moderate storm (Hs 5.0 m, gusts 86 km/h)	France 3 Nouvelle-Aquitaine + ERA5 reanalysis	✓

Out of these 17 events, 6 (marked ✓) are instrumentally constrained with contemporaneous tide-gauge, ERA5 wave and wind records suitable for the multi-frequency coupling test of §4.5. Pre-instrumental events (1936, 1977) and events known only from press releases or administrative declarations are included for completeness but are not used in quantitative tests.

---

13 Appendix B — Energetic balance of the Ferret tidal channel

Quantity	Value	Units	Source
Tidal prism (spring tide, coef 100)	384×10^6	m^3 per half-cycle	SIBA
Average flow rate	17 800	$m^3 \cdot s^{-1}$	derived
Peak velocity in channel	2.0	$m \cdot s^{-1}$	Balouin & Mallet 2007
Section area at peak	~8 000	m^2	400 m × 20 m
Bed shear stress at peak	12.3	Pa	Cf = 0.003
Critical Shields stress (200 µm)	0.12	Pa	Shields 1936
Shields ratio τ/τ_c	100	dimensionless	derived
Peak sediment transport (MPM extended)	400-4 000	$kg \cdot s^{-1} \cdot m^{-1}$	Meyer-Peter-Müller 1948
Peak sand transport	20 000-200 000	$m^3 \cdot d^{-1}$	derived
Observed Hortense pit deepening rate	58 000	$m^3 \cdot yr^{-1}$	BRGM 2019 + France 3 NA 2024
Peak/observed ratio	~300	dimensionless	derived
Expected v_{2024} per Q = v·S	1.33	$m \cdot s^{-1}$	conservation
Expected $\tau_{bed,2024}$	5.4	Pa	derived
Expected scour rate	asymptotically decreasing	—	theoretical
Observed scour rate	accelerating	—	empirical discrepancy

The peak transport capacity exceeds the observed deepening rate by two orders of magnitude; energy is not the constraint. The constraint is the **sediment mobilization law** at the pit base, which the energetic analysis suggests is being modified by one of the mechanisms in §5.

14 Appendix C — Mitigation cost structure (detailed)

Approach	Unit cost (€/m)	Lifetime (yr)	Mechanism addressed	Reversibility	ESG score	Primary source
Hard rock dike	≥ 100 000	30-50	Passive blocking only	0 %	Low	CEREMA 2015 guide, standard rock-armouring
Sediment recharge	~500	2	Mass-supply only	100 %	Medium	SIBA SLGBC 2017-2020 tenders
Ganivelle (Brémontier)	20-40	15-20	Karman, energy, creep, hydraulic	100 %	High	ONF operational data 2000-2024
Geotextile submerged breakwater	500	30	Wave energy dissipation	80 %	Medium	Koerner 2012; Baltic ports case studies
Fluvial tunage sub-aquatic	100-300	30-50	Submerged dissipation + biological substrate	90 %	High	Agence Eau Adour-Garonne field data
Oyster biogenic reef	20-40 €/m²	Centennial	Rugosity + sediment trap + auto-cementation	100 %	Very high	IFREMER reef restoration programs
Eelgrass restoration (Zostera noltei)	20-100 €/m²	Decadal	Rhizome stabilization + wave attenuation	100 %	Very high	Saint-Brieuc Bay; Arcachon Bay historical

15 Appendix D — Municipal water supply wells (Lège-Cap-Ferret)

Five wells are registered with the French national groundwater database (Hub'Eau BNPE) for the commune of Lège-Cap-Ferret, with combined withdrawal of 1.9×10^6

$m^3 \cdot yr^{-1}$ over 2015-2024. Precise locations are cross-referenced with the BSS BRGM borehole database:

#	Name (BNPE)	BSS code	Lat °N	Lon °E	Depth (m)	Aquifer captured
1	CLAOUEY 2	BSS001ZCUZ	44.74712	−1.18298	278	Plio-Miocène / upper Oligocène
2	AU BOURG LÈGE	BSS001ZCXW	44.79446	−1.14821	280	idem
3	LES JACQUETS	BSS001ZDGH	44.72693	−1.21482	453	Oligocène captif
4	LES EMBRUNS	BSS001ZCVK	44.75220	−1.19032	505	Oligocène captif
5	LES VIVIERS	BSS001ZCVH	44.73756	−1.19661	533	Eocène+Oligocène captif

Source precision: WFS BRGM BSS paginated query (715 boreholes in Cap-Ferret bounding box). BNPE publishes only the commune centroid (44.725°N, −1.223°E), consistent with regulatory confidentiality.

Observation critical for H4 testing: The Pointe subsidence cluster (44.640°N, −1.260°E) is 9.8 km to 18.7 km from the five AEP wells. No well is within 5 km of the cluster. EGMS signature around each well is quasi-null (median +0.50 to +1.15 $mm \cdot yr^{-1}$) with the single exception of the Viviers well (median −0.65 $mm \cdot yr^{-1}$ within 300 m), with amplitude **12× weaker** than the Pointe cluster.

---

16 Appendix E — Deep boreholes in the Cap-Ferret area (BSS BRGM paginated)

The Cap-Ferret bounding box contains 715 boreholes in the BSS database, of which 211 exceed 50 m depth. The deepest ten are summarized below:

BSS id	Reference	Depth (m)	Probable type	Reservoir target
BSS004LNDS	LNDS/X	4 990	Petroleum exploration	Crétacé / Jurassique
BSS001ZDGL	08257X0081/ CBY5DG	4 912	Cassy 5 DG	Campano-Maastrichtien
BSS004LNDR	LNDR/X	4 890	Petroleum exploration	idem
BSS001ZDGF	08257X0076/ CBY-4D	4 762	Cassy 4 D	idem
BSS001ZZNZ	08493X0019/LAS1	4 598	Les Acacias 1 (La Teste)	idem
BSS001ZDEF	08257X0028/ GUT1	4 593	Guttenberg 1	idem
BSS001ZZPK	08493X0029/F3	4 589	— (fiche 37 KB)	idem
BSS001ZDGJ	08257X0079/ PEGASE	4 435	PEGASE 1D / PGA 1D	idem
BSS001ZDFE	**08257X0051/ LVE4**	**4 364**	**Lavergne 4 — historical concession well-head**	**Purbeckien**
BSS001ZDFW	08257X0067/ CBY1DG	4 225	Cassy 1 DG	Campano-Maastrichtien

Context: The Lavergne concession (ESSO-REP 1962-1994, continued by Vermilion 2009-2029) targeted the Purbeckien Crétacé inférieur reservoir at ~3 200 m TVD. Production is declared at ~11 t/d post-2009, with water-drive reinjection (Vermilion 2022 concession grant). The LVE-1 well is deviated from the Pointe Cap-Ferret surface location toward the offshore area.

Mass-balance constraint for H4b (Lavergne): Under Biot conservation of pore water applied to the realistic envelope of net extraction (V_{net} = 0.4 to 5.6 × 10^6 m^3 depending on Esso production records and Vermilion water-drive reinjection ratios), the Geertsma (1973) reservoir-compaction prediction **underpredicts the observed Pointe surface signal by a factor of 50 to 220** — i.e. the Lavergne reservoir alone accounts for ≤ 2 % of the observed subsidence. The Lavergne mechanism (sub-hypothesis H4b) is therefore **falsified as the dominant source**. It cannot be excluded as a marginal contributor (< 2 %). This is geometrically consistent with the Geertsma bowl geometry, which places the maximum subsidence offshore of the well-head — currently unmeasurable due to the absence of persistent scatterers on the intertidal Banc d’Arguin (corner-reflector deployment required per §5.4).

---

17 Appendix F — Dredging and clapage operations 2002-2017 (SIBA, via BRGM 2019)

The Annex 1 of BRGM 2019 (p. 49-50) lists 40+ sediment operations in the Arcachon bay inlet between 2002 and 2017. Three operations exceed 1 × 10^6 m^3 each:

#	Commune	Start	End	Source	Destination	Volume (m^3)
1	**La Teste-de-Buch**	Jan 2003	Feb 2003	Banc de Bernet	Plages du Pyla (Nord)	**1 100 000**
2	**Lège-Cap-Ferret**	Nov 2003	Feb 2004	Aval chenal Piquey : Banc de La Vigne	Clapage au jusant zone nord flèche Mimbeau + clapage au flot zone sud Pointe Cap-Ferret	**1 000 000**
3	**Lège-Cap-Ferret**	Nov 2004	Feb 2005	Amont chenal Piquey : Banc de Jane Blanc	idem (jusant Mimbeau + flot Pointe)	**1 000 000**

Total 2003-2005 = 3.1 × 10^6 m^3 redistributed by hydraulic clapage.

Clapage technique: Sediment dredged at one site and released in open water during a precise tidal phase (flood or ebb) allows tidal currents to redistribute the sediment naturally. The BRGM 2019 report acknowledges (p. 38) that “detailed knowledge of the operations carried out” would be necessary to evaluate whether the post-2005 pit evolution is linked to these clapage operations. The detailed temporal and spatial characterization of the clapage operations has not been publicly released.

Hortense pit void volume evolution (BRGM 2019 Fig. 25):

Year	Cumulative void volume below −16 m CM (m^3)
2003	~290 000 (pre-clapage)
2004	~280 000 (during clapage)
2005	**~220 000** (minimum — maximum infill)
2006	~290 000 (back to baseline)
2007	~360 000
2009	~390 000
2010	~450 000 (pit merger below −16 m)
2012	~470 000
2015	**~540 000 (+145 % vs 2005)**

This non-linear post-dredging trajectory is exactly what hypothesis H2 predicts.

18 Appendix G — Link between historical bio-engineering and the four mechanisms

Mechanism (peer-reviewed literature)	Palisade addresses via	Original source
Karman vortex street	Strouhal 0.2 vortices decelerate suspended sand, promote deposition	Standard fluid mechanics textbook
Cyclic energy dissipation 0.05-0.3 Hz (H3)	Partial reflection + friction reduce γ below Youd threshold 10^{-4}	Youd 1972; Seed & Idriss 1971
Lateral creep kinematic constraint	10-30 kN/m² horizontal bracing from embedded piles	Meyerhof 1976; Gazetas 1983
Hydraulic barrier + capillary cohesion	Reduces drainage velocity, breaks preferential piping paths (H1)	Fredlund & Rahardjo 1993; Burnett et al. 2006

All four mechanisms are empirically embedded in the 240-year validation of the Brémontier technique. The contribution of this paper is not to discover them, but to recognize their simultaneous operation within a single low-cost intervention.

Word count: ~9 000 words (body) + appendices.

Submitted for open peer review.

Corresponding author: B. Gasque, independent researcher, Claouey, Lège-Cap-Ferret, France.

Conflict of interest declaration: the author declares no financial conflict of interest. All research was conducted on personal time with personal resources on open hardware. No commission from any governmental, commercial, or non-governmental entity.

License: This preprint is released under CC-BY 4.0. Data and code are archived on Zenodo with permanent DOI: https://doi.org/10.5281/zenodo.19815152 (CC-BY 4.0).